Journal of Medicinal Chemistry

pubs.acs.org/jmc

Drug Annotation

Discovery and Preclinical Pharmacology of INE963, a Potent and Fast-Acting Blood-Stage Antimalarial with a High Barrier to Resistance and Potential for Single-Dose Cures in Uncomplicated Malaria

Benjamin R. Taft,* Fumiaki Yokokawa,* Tom Kirrane, Anne-Catherine Mata, Richard Huang, Nicole Blaquiere, Grace Waldron, Bin Zou, Oliver Simon, Subramanyam Vankadara, Wai Ling Chan, Mei Ding, Sandra Sim, Judith Straimer, Armand Guiguemde, Suresh B. Lakshminarayana, Jay Prakash Jain, Christophe Bodenreider, Christopher Thompson, Christian Lanshoeft, Wei Shu, Eric Fang, Jafri Qumber, Katherine Chan, Luying Pei, Yen-Liang Chen, Hanna Schulz, Jessie Lim, Siti Nurdiana Abas, Xiaoman Ang, Yugang Liu, Iñigo Angulo-Barturen, María Belén Jiménez-Díaz, Francisco Javier Gamo, Benigno Crespo-Fernandez, Philip J. Rosenthal, Roland A. Cooper, Patrick Tumwebaze, Anna Caroline Campos Aguiar, Brice Campo, Simon Campbell, Jürgen Wagner, Thierry T. Diagana, and Christopher Sarko

Cite This: *J. Med. Chem.* 2022, 65, 3798–3813

Read Online

ACCESS | Metrics & More | Article Recommendations | Supporting Information

ABSTRACT: A series of 5-aryl-2-amino-imidazothiadiazole (ITD) derivatives were identified by a phenotype-based high-throughput screening using a blood stage *Plasmodium falciparum* (*Pf*) growth inhibition assay. A lead optimization program focused on improving antiplasmodium potency, selectivity against human kinases, and absorption, distribution, metabolism, excretion, and toxicity properties and extended pharmacological profiles culminated in the identification of **INE963** (**1**), which demonstrates potent cellular activity against *Pf* 3D7 (EC_{50} = 0.006 μM) and achieves "artemisinin-like" kill kinetics *in vitro* with a parasite clearance time of <24 h. A single dose of 30 mg/kg is fully curative in the *Pf*-humanized severe combined immunodeficient mouse model. **INE963** (**1**) also exhibits a high barrier to resistance in drug selection studies and a long half-life ($T_{1/2}$) across species. These properties suggest the significant potential for **INE963** (**1**) to provide a curative therapy for uncomplicated malaria with short dosing regimens. For these reasons, **INE963** (**1**) was progressed through GLP toxicology studies and is now undergoing Ph1 clinical trials.

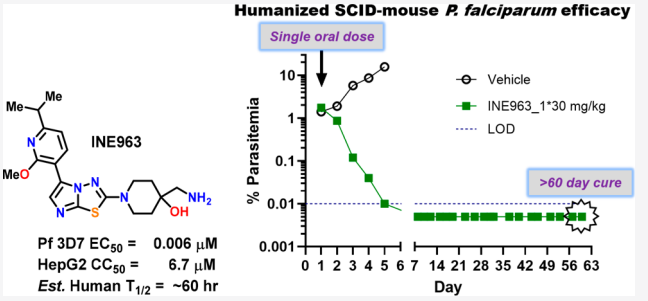

INTRODUCTION

Malaria is the world's most prevalent infectious and life-threatening disease, caused by the protozoan parasite *Plasmodium* that is transmitted to human hosts by female *Anopheles* mosquitoes. In 2019, there were an estimated 229 million cases and 409,000 deaths, mostly affecting children aged under 5 years. Nearly half of the world's population is at risk of malaria infection. Most malaria cases and deaths occur in sub-Saharan Africa, while South-East Asia, Eastern Mediterranean, Western Pacific, and the Americas are also at risk. Currently artemisinin-based combination therapy is recommended as a first-line treatment for uncomplicated malaria caused by *Plasmodium falciparum* (*Pf*) and has proved effective in reducing the disease burden.[1]

Artemisinin derivatives are highly potent and fast-acting antimalarials that produce rapid clinical responses to treatment. However, there has been an increasing number of reports of artemisinin-resistant malaria in the Greater Mekong subregion,[2] and in addition, resistance against partner drugs such as mefloquine and piperaquine is already widespread.[3,4] Furthermore, recent reports of dihydroartemisinin-piperaquine treatment failures have been documented.[5] The emergence of

Received: November 21, 2021
Published: March 1, 2022

https://doi.org/10.1021/acs.jmedchem.1c01995
J. Med. Chem. 2022, 65, 3798–3813

artemisinin resistance is a real threat to malaria treatment and elimination efforts worldwide.[6] As a consequence, there is still an urgent need to identify new antimalarial compounds that can be added to or substitute the current artemisinin-based therapies. The artemisinin family has a short half-life and needs to be combined with a longer-acting partner drug for complete clearance of parasites.[7] Therefore, our goal at the Novartis Institute for Tropical Diseases (NITD) is to identify a fast-acting antimalarial compound from a novel chemotype with activity against known resistance mutations and which will also have the potential for single-dose cures.[8] Novel antimalarial chemotypes are expected to have a different mode of action to current drugs, and thus no cross resistance. In recent years, phenotype-based approaches have proven successful for the identification of new antimalarial chemotypes with novel modes of action, and as a result, several lead candidates such as KAE609,[9] KAF156,[10] DSM265,[11] MMV048,[12] SJ733,[13] M5717,[14] and ZY19489[15] have been advanced to clinical trials to show activity in patients.

In our continued research efforts at NITD to identify new antimalarial leads, our phenotypic screening campaigns and subsequent follow-up structure−activity relationship (SAR) studies around various hit series resulted in the identification of the 5-aryl-2-amino-imidazothiadiazole (ITD) lead compound, **2**, which displayed modest potency (EC_{50} of 0.27 μM) against the cultured parasite *Pf* 3D7 (Figure 1). During optimization

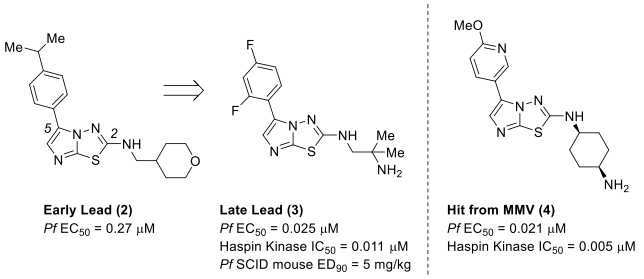

Figure 1. Early and late lead 5-aryl-2-amino-ITD antiplasmodium compounds discovered by Novartis and 5-aryl-2-amino-ITD hit disclosed by MMV.

of the scaffold, the late-lead compound **3** was rapidly identified with improved potency (EC_{50} = 0.025 μM) and excellent *in vivo* pharmacokinetics. Compound **3** demonstrated a single dose ED_{90} of 5.3 mg/kg against *Pf* infected mice and a similar speed-of-action to artemisinin. In addition, a single dose of 50 mg/kg was fully curative with no observed recrudescence after 60 days (Table 8). During our early studies of the 5-aryl-2-amino-ITD chemical series, Medicines for Malaria Venture (MMV) independently conducted a high-throughput screen of a chemical library consisting of more than 250,000 compounds against blood-stage *Pf*.[16] Structures of 15 validated hits were disclosed, including the 5-aryl-2-amino-ITD analog **4**. Compound **4** was resynthesized in our laboratories for biological characterization and confirmed potent antiplasmodium activity with an EC_{50} of 0.021 μM.

Despite the promising *in vitro* and *in vivo* antimalarial profiles of this ITD series, we were concerned about the off-target selectivity given that a related chemical series of 5-aryl-2-amino-ITDs are described in the patent literature as potent inhibitors of human kinases (e.g., FLT3, PIK3CA, and PIM1).[17,18] In addition, early animal toxicology studies of **3** in rats and dogs indicated that there was not an adequate safety margin to progress this compound further. Thus, to assess the broader human kinase inhibition profile of **3**, the binding affinities to 468 human kinases were tested at a 10 μM concentration. Compound **3** inhibited 53 out of 468 human kinases at <10% of control (Figure 6), which we suspected was directly impacting the rat and dog toxicology findings and was likely a major factor resulting in the narrow safety margins observed.

Additionally, we observed that the *in vitro* potency of **3** decreased over time after multiple rounds of testing (EC_{50} = 1.16 μM), indicating that **3** was likely degrading in DMSO stock solution. Chemical stability analysis revealed that the crystalline malate salt of **3** degraded over 24 h to 2.6% and 77.4% of the parent in pH 6.8 and fasted state simulated intestinal fluid (FaSSIF) solutions, respectively. Although **3** was chemically stable in the solid state, the solution instability was deemed a development risk. An additional analysis using 2D NMR elucidated the structure of the degraded product **C**/**D**, which suggested tautomerization of the 2-amino-ITD moiety to the 2-imino-thiazolidine **A**. This tautomer **A** can be a trigger of nucleophilic cyclization by the terminal amine and result in spiro-cycle **B**, thereby leading to the degradation product **C**/**D** as illustrated in Figure 2.

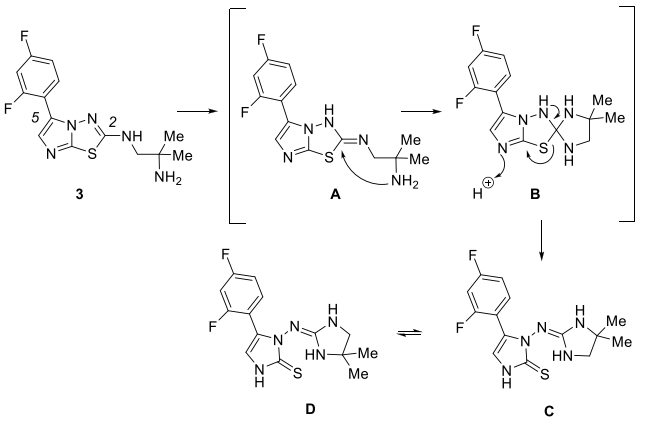

Figure 2. Putative mechanism of tautomerization and degradation of **3**.

Therefore, we undertook lead optimization of the 5-aryl-2-amino-ITD series to address the issues of chemical stability and human kinase promiscuity, while maintaining or improving the desirable pharmacological and safety properties. Herein, we describe a phenotype-based SAR study around the 5-aryl-2-amino-ITD scaffold with a focus on selectivity against human kinases and optimization of physiochemical and absorption, distribution, metabolism, and excretion (ADME) properties suitable for a single-dose cure therapy in uncomplicated malaria.

RESULTS AND DISCUSSION

The proposed mechanism of tautomerization and chemical degradation suggested that removing the hydrogen of the 2-N(H)R linker would improve the chemical stability of the 5-aryl-2-amino-ITD scaffold. In addition, we had observed early on that related compounds which replaced the 2-N(H)R with a 2-N(Me)R linker were more chemically stable and maintained good potency. We were then pleased to find that the cyclic 4-methyl-4-amino-piperidine analog, **5**, provided a

https://doi.org/10.1021/acs.jmedchem.1c01995
J. Med. Chem. 2022, 65, 3798−3813

2.5-fold increase in antiplasmodium activity along with increased chemical stability. In addition, replacement of the 2-amino-linker with a 2-carbon-linker, **6** and **7**, was also tolerated albeit with slightly lower potency. It is hypothesized that preventing tautomerization as well as the increasing rigidity of the side chain both improve chemical stability. Unexpectedly, replacement of the 2-amino-linker with an ether or thioether resulted in a dramatic loss in antiplasmodium activity. Considering the best potential to combine chemical stability, antiplasmodium potency, and synthetic tractability, **5** was selected as a starting point for further optimization (Table 1).

Table 1. *In Vitro* Antiplasmodium Activity of 2-Amino and 2-Carbon Linked ITD Analogs

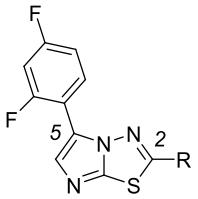

cpd	R	*Pf*3D7 EC_{50} (μM)[a]	Chemical stability
3	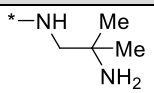	0.025	×
5	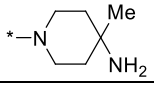	0.009	√
6	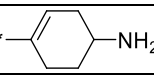	0.033 (n=2)	√
7	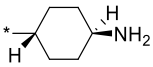	0.045 (n=1)	√

[a]EC_{50} values are given as average potency values in the *Pf* 3D7 assay ($n \geq 3$). Standard control mefloquine has an EC_{50} value of 0.034 uM.

SARs for *Pf* 3D7 Activity and Selectivity against Human Haspin Kinase. We first investigated the antiplasmodium SAR as well as the human kinase selectivity by systematic modifications of the 2,4-difluorobenzene moiety of **5** (Table 2). Haspin kinase proved to be the most sensitive and was used as the benchmark for selectivity comparisons. The IC_{50} value of late lead compound **3** against Haspin was determined to be 0.011 μM. In addition, the screening hit **4** published by MMV, and our starting point **5**, showed a similar Haspin inhibitory activity compared to **3**. Replacement of the 2-F with 2-Me (**8**) and 2-OMe (**9**) reduced the Haspin inhibition to IC_{50}'s of 1.28 and 1.74 μM, respectively, while maintaining antiplasmodium activity. Exchanging the 4-F to 4-OMe (**10**) decreased Haspin selectivity. Transposition of the 4-F to 6-F to give the 2,6-disubstituted analog (**11**) resulted in a 10-fold drop in antiplasmodium potency, presumably due to an increase in the biaryl dihedral angle (based on the observed orientation of compound **5** in the X-ray structure; Figure 3). The 3-OMe, 2-F analog (**12**) had a similar potency and selectivity as compared to **9**, supporting the observation that the 2-OMe or 3-OMe substituent improves selectivity against Haspin. Replacement of the 2-OMe substituent with sterically larger groups such as −OEt (**13**) and −O-^{i}Pr (**14**) resulted in further reducing the Haspin inhibition while retaining potency. However, shifting the position of the ether oxygen of **13** to 2-CH_2OMe (**15**) decreased potency (EC_{50}, 0.11 μM). The 2-OCH_2CH_2OMe polar side chain (**16**) also led to weaker potency. The dihydrobenzofuran (**17**) had similar antiplasmodium potency and Haspin inhibitory activity to **9**, while the indole (**18**) and *N*-methylindole analog (**19**) were less potent. Introduction of the pyridine nitrogen to **9** yielded the 2-fluoro-6-OMe pyridine (**20**), which had similar antiplasmodium activity but 2−3 fold lower selectivity against Haspin. The regioisomeric 2-OMe-pyridine analog (**21**) further decreased selectivity against Haspin. Heteroaromatics such as pyrimidine and thiazole were significantly less potent (**22**−**26**).

Several nonaromatic moieties were also examined. The *tert*-butylacetylene analog (**27**) had good antiplasmodium potency and maintained good selectivity against Haspin, however the cyclopropylacetylene (**28**) dropped the potency by 3-fold and the propargyl alcohol (**29**) was not tolerated. Cyclohexene (**30**) retained good antiplasmodium potency, but lost Haspin selectivity. Conversely, 4,4-difluorocyclohexane (**31**) and cyclopentane (**32**) moieties led to a significant loss of the antiplasmodium activity.

Compound **9** was then selected for *in vitro* profiling where it exhibited improved chemical stability in FaSSIF solution (compared to **3**) and retained good metabolic stability (Table 3). Compound **9** also demonstrated a lower affinity against a small panel of selected human kinases in addition to Haspin (CDK7, FLT3, KIT, PIM-1,2,3), suggesting that the 2-OMe-aryl substituent reduces overall human kinase promiscuity.

During this SAR study at the 5-position of the ITDs, an X-ray cocrystal structure of the 2,4-difluorobenzene compound **5** with Haspin was solved with a resolution of 1.8 Å (Figure 3). Interestingly, the ITD core is bound to the hinge region via one H-bond between the 7-nitrogen atom and G608 (2.9 Å) and a σ−hole interaction of sulfur with G609 (3.4 Å). The costructure also shows a clear salt bridge interaction between D611 (2.8 Å) of the lower hinge and the ammonium cation of **5**. This binding mode of the ITD core projects the 2,4-difluorobenzene ring in a coplanar fashion which binds to Haspin in a hydrophobic pocket with close contact (<3.5 Å) of nearby residues and sheds light on our observed SAR of the 2-OMe or 3-OMe aryl analogs. This hydrophobic pocket likely causes a steric clash with 2-OMe or 3-OMe aryl ITD analogs, mitigating affinity to and inhibition of Haspin kinase while still allowing potent antiplasmodium activity (**9** and **12**). This theory for antiplasmodium vs human kinase selectivity is further exemplified by the good potency of 4-OMe analogs in both *Plasmodium* and Haspin assays (**10**), where there appears to be more room in the Haspin binding pocket. To further probe this binding mode, we introduced a methyl group directly to the 6-position of the ITD core to obtain **33**, which led to a significant loss of both antiplasmodium and Haspin activities. Similarly, additional minor modifications of the ITD core resulted in significant loss of antiplasmodium potency, for example, the replacement of the nitrogen with carbon at the 3-position (i.e., imidazothiazole) **34** (Figure 4).

Optimization of the 2-Amino-Alkyl Side Chain of ITDs. Although **9** addressed the issues of the chemical stability and kinase promiscuity, we saw opportunities to further improve upon the potential cardiosafety risk (hERG Qpatch IC_{50} = 2.4 μM) and absorption, distribution, metabolism, excretion, and toxicity properties. Consequently, the next phase of optimization focused on modifications to the 2-

https://doi.org/10.1021/acs.jmedchem.1c01995
J. Med. Chem. 2022, 65, 3798−3813

Table 2. SAR of the 5-Position of ITDs

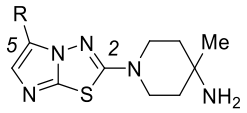

cpd	R	*Pf*3D7 EC_{50} (μM)[a]	Haspin IC_{50} (μM)	cpd	R	*Pf*3D7 EC_{50} (μM)[a]	Haspin IC_{50} (μM)
3	-	0.025	0.011	**19**		0.13	-
4	-	0.021	0.005	**20**		0.014	0.69 (n=2)
5		0.009	0.003	**21**	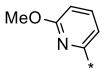	0.028 (n=2)	0.078 (n=2)
8	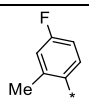	0.022	1.28 (n=2)	**22**	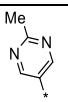	3.17	-
9	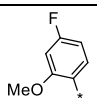	0.017	1.74	**23**	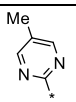	2.33	-
10		0.045	0.032 (n=1)	**24**		0.40	-
11	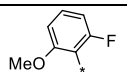	0.22	-	**25**	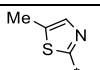	0.44	-
12	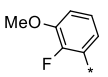	0.028	0.77 (n=2)	**26**	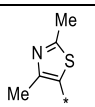	0.41	-
13	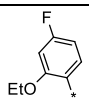	0.009	4.96 (n=2)	**27**		0.067	4.04 (n=2)
14	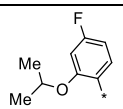	0.013	5.31 (n=2)	**28**		0.2	-
15	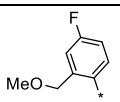	0.10	-	**29**		>10	0.14 (n=1)
16	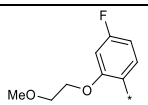	0.079	8.07 (n=1)	**30**		0.02	0.045 (n=2)
17		0.017	1.33 (n=2)	**31**	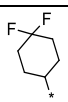	0.34	-
18		0.052	0.20 (n=1)	**32**		0.15	-

[a]EC_{50} and IC_{50} values given as averages ($n \geq 3$ unless otherwise noted). Standard control mefloquine has an EC_{50} value of 0.034 uM.

https://doi.org/10.1021/acs.jmedchem.1c01995
J. Med. Chem. 2022, 65, 3798−3813

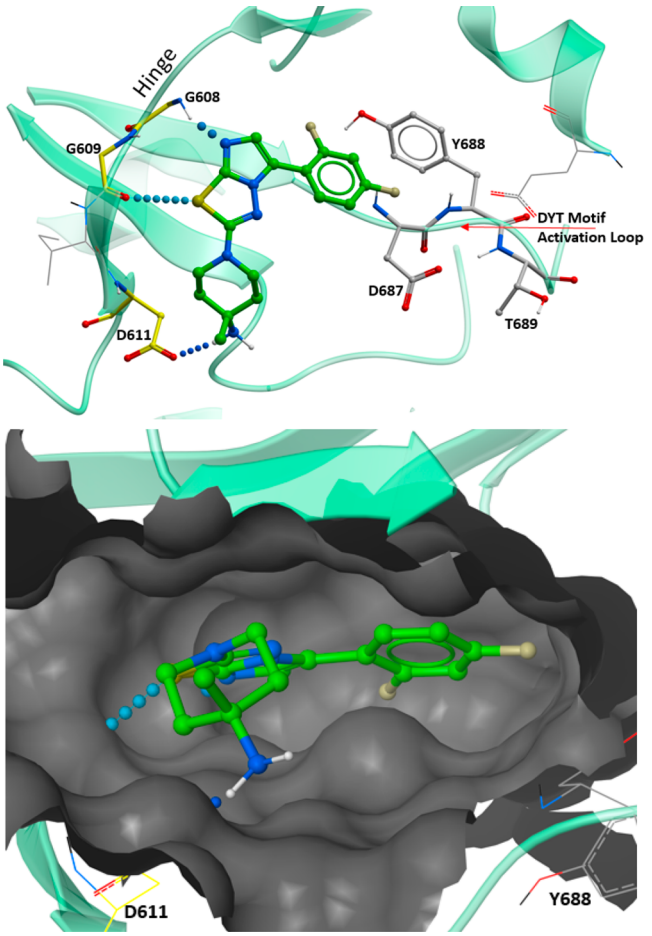

Figure 3. X-ray cocrystal structure of **5** (green) with Haspin kinase. PDB code is 7SQM.

amino-alkyl side chain of the ITD series with an emphasis on reducing the lipophilicity and pK_a, while maintaining antiplasmodium activity. Introduction of a hydroxyl group adjacent to the basic amino group led to several vicinal amino-alcohol substituted piperidine analogs, most of which displayed a decreased hERG inhibition with IC_{50}'s > 20 μM. Enantiomers **35** and **36** displayed a slight improvement in cell LipE (lipophilic ligand efficiency, LipE = pEC_{50} − log $D_{7.4}$) with a lower pK_a compared to **9**, while there is no enantiomeric preference for antiplasmodium activity. Both **35** and **36** have acceptable liver microsomal stability and exhibited good *in vivo* oral exposure profiles in rats (Table 4). Further reduction of lipophilicity by removing the 4-methyl group of the piperidine ring led to *trans*-amino-alcohol enantiomers, **37** and **38**, which displayed an improvement in cell LipE while maintaining good metabolic stability and reduced pK_a, however lower oral exposure was observed in rats with **37** presumably due to a slight drop in permeability and volume. The corresponding *cis*-amino-alcohol piperidine isomers, **39** and **40**, were slightly less potent on *Plasmodium*, despite their higher basicity. Trans-position of the amino-alcohol provided another enantiomeric pair of *cis*-amino-alcohol analogs, **41** and **42**, which showed similar antiplasmodium activity (EC_{50} = 0.029 μM) with lower basicity (pK_a 7.8), however both enantiomers increased the hERG inhibition (IC_{50} < 20 μM) and **41** had low oral exposure in rats despite its good metabolic stability. The corresponding *trans*-amino-alcohol analogs, **43** and **44**, further reduced the pK_a to 7.5, however the *Plasmodium* potency was also slightly

Table 3. Summary of Key Data for 9 for Comparison to 3

	3	9
	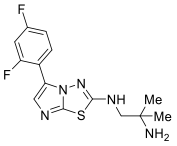	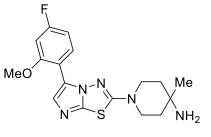
MW, tPSA, cLogP, pKa	323.4, 66.0, 2.91, 9.3	361.4, 66.5, 1.76, 8.9
Pf 3D7 EC_{50} (μM)	0.025	0.017
HepG2 CC_{50} (μM)	18	31
Kinase Kds CDK7/FLT3/ Haspin/KIT/ PIM1/PIM2/ PIM3 (μM)	0.2/0.1/ 0.01/1.5/ 0.2/0.2/0.1	12.0/0.6/ 1.7/2.4/ 1.8/7.4/26.0
% chemical degradation (in FaSSIF at 37 °C for 72 h)	7.8 % (malate salt)	0.9 % (formate salt)
H/R/M Liver Microsome CL (μL/min/mg)	<25/32/<25	<25/31/38
hERG Qpatch IC_{50} (μM)	22	2.4

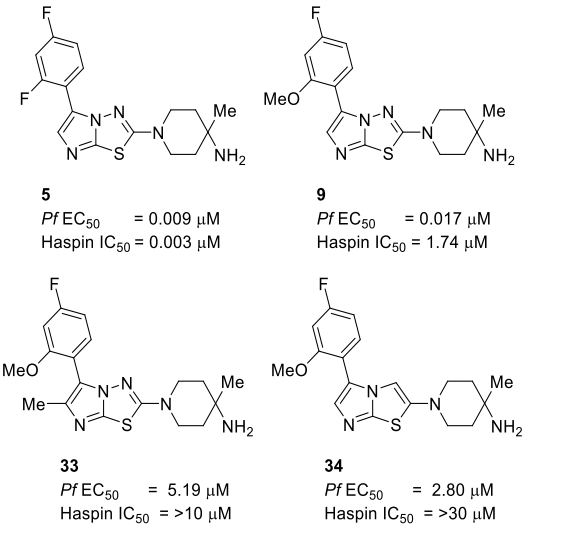

Figure 4. Key SAR of ITD-analogs on HASPIN kinase and *Pf*.

diminished (EC_{50}'s = >0.030 μM). Replacement of the hydroxyl group in **39** and **40** with fluorine led to *cis*-4-amino-3-fluoro-piperidine isomers **45** and **46**, which decreased cellular LipE and increased the hERG inhibition. The corresponding *trans*-4-amino-3-fluoro-piperidine analog **47** further diminished the *Plasmodium* potency. Ring contraction led to *cis*-4-amino-3-hydroxy-pyrrolidine and 3-amino-3-hydroxymethyl pyrrolidine analogs as enantiomeric pairs (**48** and **49**, **50** and **51**). While these pyrrolidine analogs had

https://doi.org/10.1021/acs.jmedchem.1c01995
J. Med. Chem. 2022, 65, 3798−3813

Table 4. SAR of the 2-Amino-alkyl Group[a]

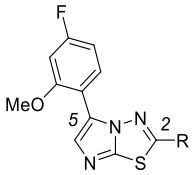

Cpd	R	*Pf* 3D7 EC_{50} (μM)	Qpatch hERG IC_{50} (μM)	logD pH 7.4	LipE (cell)	pKa	H/R LM CL_{in} (μL/min/mg)	Rat C_{max} (nM) @10 mg/kg	Rat AUC (nM*h) @10 mg/kg
9	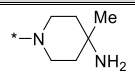	0.017	2.4	2.0	5.8	8.9	-	-	-
35 (peak-1)	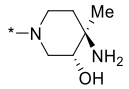	0.02	>30	1.8	5.9	8.4	<25 / 28	2,401	37,977
36 (peak-2)		0.02	>30	1.7	6.0	8.3	<25 / <25	1,759	33,773
37 (peak-1)	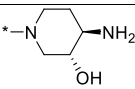	0.021	21.3	1.5	6.2	8.3	<25 / <25	402	3,956
38 (peak-2)		0.02	>30	1.3	6.4	8.3	<25 / <25	-	-
39 (peak-1)	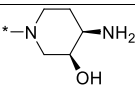	0.046	>30	0.9	6.4	8.7	-	-	-
40 (peak-2)		0.029	>30	0.9	6.6	8.6	-	-	-
41 (peak-1)	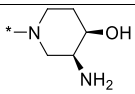	0.029	14.4	2.1	5.4	7.8	<25 / 26.9	669	8,251
42 (peak-2)		0.029	9.2	2.0	5.5	7.8	<25 / 51.7	-	-
43 (peak-1)	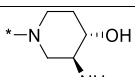	0.031	28.5	1.6	5.9	7.5	-	-	-
44 (peak-2)		0.038	>30	1.7	5.7	7.5	-	-	-
45 (peak-1)	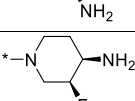	0.028	8.8	2.1	5.5	7.8	-	-	-
46 (peak-2)		0.026 (n=2)	13.9	2.3	5.3	7.8	-	-	-
47 (*rac.*)	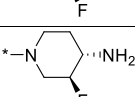	0.082	-	2.4	4.7	7.2	-	-	-
48 (peak-1)	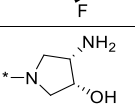	0.062	>30	1.6	5.6	7.4	-	-	-
49 (peak-2)		0.067	>30	1.7	5.5	7.4	-	-	-
50 (peak-1)	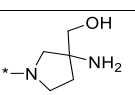	0.066	>30	1.7	5.5	7.3	-	-	-
51 (peak-2)		0.045	28.3	1.6	5.7	7.3	-	-	-
52 (peak-1)		0.027	17.8	1.3	6.3	8.5	<25 / <25	762	8,987
53 (peak-2)	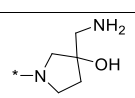	0.024	21.9	1.1	6.5	8.4	<25 / <25	-	-
54	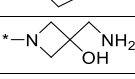	0.056	>30	1.2	6.1	8.0	-	-	-
55	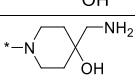	0.021	18.5	1.4	6.3	8.8	<25 / 50.1	2,268	41,767
56	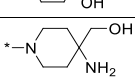	0.017	17.7	1.9	5.9	8.2	<25 / 25.1	1,367	20,198
57	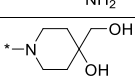	0.49	-	3.2	3.1	-	-	-	-
58	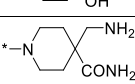	0.130	-	1.5	5.4	7.3	-	-	-
59	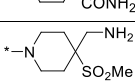	0.31	-	2.2	4.3	6.9	-	-	-

https://doi.org/10.1021/acs.jmedchem.1c01995
J. Med. Chem. 2022, 65, 3798−3813

Table 4. continued

Cpd	R	*Pf* 3D7 EC_{50} (μM)	Qpatch hERG IC_{50} (μM)	logD pH 7.4	LipE (cell)	pKa	H/R LM CL_{in} (μL/min/mg)	Rat C_{max} (nM) @10 mg/kg	Rat AUC (nM*h) @10 mg/kg
60	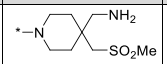	0.044	-	1.8	5.6	-	-	-	-
61	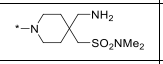	0.053	-	2.2	5.1	8.0	-	-	-
62	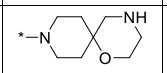	0.022	-	2.7	5.0	-	-	-	-
63	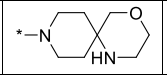	0.062	-	2.7	4.5	7.1	-	-	-

[a]Peak-1: Fast-eluting isomer from chiral HPLC. Peak-2: Slow-eluting isomer from chiral HPLC. HLM: Human liver microsomes. RLM: Rat liver microsomes. C_{max}, AUC: mean blood concentration time profile from oral administration to rats at 10 mg/kg.

reduced basicity (pK_a < 8), they also showed lower *Plasmodium* potency (EC_{50}'s = >0.045 μM). Transposition of the −OH and $-NH_2$ in **50** and **51** led to 3-hydroxy-3-aminomethyl pyrrolidine analogs, **52** and **53**, which increased the antiplasmodium activity (albeit with higher pK_a > 8), however oral exposure of **52** was not comparable to the 3,4-hydroxy-aminopiperidine analogs **35** and **36**.

To minimize synthetic complexity and avoid the chirality of the 3,4-hydroxy-amino piperidines and pyrrolidines, symmetrical cyclic hydroxy amines were examined. The 3-hydroxy-3-aminomethyl-azetidine analog **54** had diminished *Plasmodium* potency, however the 4-hydroxy-4-aminomethyl-piperidine analog **55** displayed equipotency with an improved cell LipE, as compared to **35** and **36**. Transposition of the hydroxyl and amino groups of **55** led to a lower pK_a while maintaining good potency and high cell LipE (**56**). Compound **55** exhibited a comparable oral PK profile in rats to **35** and **36**, despite its slightly higher rat microsomal clearance, whereas **56** resulted in a 2-fold lower oral exposure in rats than **55**. Replacement of the basic amine in **55** with a second hydroxyl group led to a significant drop in the potency (**57**; EC_{50} = 0.49 μM), further confirming the observed SAR and hypothesis that a basic amine is required to obtain potent antiplasmodium activity.

To probe the limits of LipE and further reduce the lipophilicity of **55**, the hydroxy group was replaced with a carboxamide and methylsulfone to give **58** and **59**, which were significantly less potent on *Plasmodium* and resulted in lower cell LipEs. Homologation of **59** with a methylene carbon improved the antiplasmodium activity, but **60** was still less potent with a lower cell LipE than **55**. Replacement of the methylsulfone in **60** with a dimethylsulfonamide did not improve the potency (**61**). Finally, two cyclic analogs of **55** and **56** were prepared but displayed lower *Plasmodium* potency and lower cell LipE (**62** and **63**). Therefore, on the basis of high cellular LipE, low inhibition of hERG, good oral exposure, and low synthetic complexity (lack of the chirality), the 4-(aminomethyl)piperidin-4-ol group (**55**) was prioritized as an optimal amino-alkyl side chain for the ITD core.

Optimization of LipE and PK/PD Properties: Identification of Clinical Candidate INE963 (1). At this stage of the optimization, our attention turned back to the 5-aryl group, with the aim of further increasing the antiplasmodium potency as well oral exposure, both of which are viewed as critical properties to improve the potential for a single dose treatment. It was hypothesized that increasing lipophilicity would lead to increased tissue binding and volume of distribution (V_{ss}), thereby increasing the half-life ($T_{1/2}$) and improving *in vivo* efficacy. However, increasing lipophilicity often adversely affects metabolic stability and off-target selectivity. Therefore, our ambition was to find the most suitable substitution of the 5-aryl-group to combine with the 4-(aminomethyl)piperidin-4-ol side chain and provide a compound with balanced polarity and ideal drug-like properties. To assess the optimal properties for *in vivo* efficacy, human and rat hepatocyte clearance as well as oral exposure in rats were determined, including the ratio of 48 h concentration over *Pf* EC_{50} as a pharmacokinetic/pharmacodynamic (PK/PD) surrogate for maintaining a high parasiticidal concentration over one parasite life-cycle.

Homologation of the 2-OMe group to the 2-OEt group (**64**) slightly improved the potency but led to lower cell LipE and 2-fold lower oral exposure as compared to **55** (Table 5). Interestingly, the $C_{48\ h}/EC_{50}$ was slightly improved (10.8 vs 9.1) despite the lower exposure. Replacement of the *para*-fluoro with a methyl group provided **65**, which displayed a hERG IC_{50} of >30 μM with comparable *Plasmodium* potency to **55**. Moreover, **65** had a similar oral exposure with 2-fold higher $C_{48\ h}/EC_{50}$ ratio (18.6 vs 9.1) than **55**. It was then hypothesized that introduction of a nitrogen in the ring at the *meta*-position (adjacent to both *ortho*-OMe and *para*-Me) would mitigate lipophilicity and metabolism, while still being shielded from intermolecular interactions. We were subsequently pleased to see that **66** achieved a high cell LipE (6.4) due to improved *Plasmodium* potency and lower log *D*, albeit with lower oral exposure and $C_{48\ h}/EC_{50}$ ratio (10.9 vs 18.6) compared to **65**. Further systematic exploration of SARs at the *para*-position revealed that only lipophilic groups were tolerated and identified an isopropyl group, **INE963** (**1**), which improved antiplasmodium activity to single digit nanomolar (EC_{50} = 0.006 μM). The *para*-isopropyl group increased overall compound lipophilicity, albeit without significantly increasing *in vitro* hepatic clearance. Due to these ADME properties, **INE963** (**1**) attained a longer $T_{1/2}$ (19.2 h) with a very high $C_{48\ h}/EC_{50}$ ratio (33.3) compared to other analogs. The related 6-isopropyl-2-OEt-pyridyl analog, **67**, had similar antiplasmodium potency and exposure in rats, although with lower LipE and increased hERG inhibition (IC_{50} = 12 μM). Therefore, it was determined that the additional lipophilicity of the *ortho*-OEt group in **67** provided minimal advantage compared to **INE963** (**1**). For these reasons, and with a focus on selecting a candidate with good potential for single dose treatment in humans, it was determined that

https://doi.org/10.1021/acs.jmedchem.1c01995
J. Med. Chem. 2022, 65, 3798−3813

Table 5. SAR of the 5-Aryl Group in Combination with the 4-Hydroxy-4-aminomethyl-piperidine Side Chain

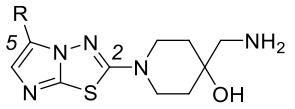

Cpd	R	*Pf* 3D7 EC_{50} (μM)	Qpatch hERG IC_{50} (μM)	logD pH 7.4	LipE (cell)	Hep CL_{int} (H/R) (μL/min/10^6 cells)	PPB (%) (H/R)	C_{max} (nM)	AUC (nM*h)	$T_{1/2}$ (h)	C_{48h} /EC_{50}
55	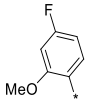	0.021	18.5	1.4	6.3	<4 / 5.5	87.5 / 81.8	2,268	41,767	12.7	9.1
64	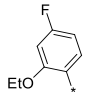	0.014	21.5	2.1	5.8	9.4 / <4	96.8 / 93.5	1,207	24,433	15.7	10.8
65	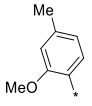	0.017	>30	1.8	6.0	8.4 / 4.9	91.5 / 87.0	2,382	48,841	14.7	18.6
66	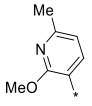	0.011	27.5	1.5	6.4	9.3 / <4	90.4 / 88.6	828	17,771	15.8	10.9
INE963 (1)	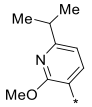	0.006	23.0	3.1	5.2	<4 / 7.1	>99 / >99	996	21,592	19.2	33.3
67	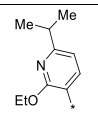	0.005	12.3	3.4	4.9	<4 / <4	>99 / >99	1,113	22,719	18.1	38.8

[a]Hep CL_{int}: *In vitro* hepatocyte clearance. PPB: Plasma protein binding. C_{max}, AUC, $T_{1/2}$: from mean blood concentration time profile of oral administration in rats at 10 mg/kg.

INE963 (1) had the best overall profile and was progressed to further biological characterization.

***In Vitro* Efficacy and Selectivity.** **INE963 (1)** was profiled in numerous *in vitro Plasmodium* blood-stage growth inhibition assays and shows excellent potency (Table 6). The EC_{50} values of **INE963 (1)** are single digit nanomolar against *Pf* 3D7 blood stages: EC_{50} = 3.0−6.0 nM. **INE963 (1)** is also potent against *P. falciparum* and *P. vivax* clinical isolates from Brazil and Uganda with EC_{50}'s ranging from 0.01 to 7.0 nM.[19,20] Additionally, **INE963 (1)** is active against >15 drug-resistant *Pf* cell lines with EC_{50}'s = 0.5−15 nM. The biological target in parasites has not been identified to date, but investigations are ongoing. The mechanism of action (MoA) appears to be novel due to the activity against multidrug-resistant *Pf* parasite lines in addition to showing a high barrier to resistance. To date, we have been unable to generate any drug-resistant mutants in selection studies using multiple protocols conducted with various *Pf* blood stage cultures *in vitro*. The *in vitro* selectivity of **INE963 (1)** for *Plasmodium* vs human cells was exemplified by approximately 1000+ fold shifts against multiple human kinase biochemical assays as well as respectable margins in multiple cell lines used for cytotoxicity assays (Table 6).

Table 6. *In Vitro* Efficacy and Selectivity of INE963 (1)

assays	**INE963 (1)** data (μM)
Pf 3D7 EC_{50} (SYBR green)	0.006
Pf 3D7 EC_{50} (3H-hypoxanthine)	0.003
Brazilian isolates[19] EC_{50} (*Pf;* SMA)	0.003 (0.002−0.005) median IC_{50} (range)
Brazilian isolates[19] EC_{50} (*P. vivax;* SMA)	0.002 (0.0005−0.007) median IC_{50} (range)
Uganda isolates[20] EC_{50} (*Pf;* SYBR green)	0.0004 (0.00001−0.0046) Median IC_{50} (range)
human kinase IC_{50} (Haspin, FLT3, PIK3CA, PIM1)	5.5, 3.6, >50, >50
cytotoxicity CC_{50} (HepG2, K562, MT4)	6.7, 6.0, 4.9

The fast-killing potential of **INE963 (1)** has been demonstrated in a *Pf* viability assay (GSK, Tres Cantos) using a limiting dilution technique to quantify the number of *Pf* 3D7 parasites that remain viable after drug treatment.[21,22] The results show no viable parasites after 24 h (5 log reduction) which is comparable to or faster than artemisinin. The *in vitro* log parasite reduction ratio for **INE963 (1)** is >8.0 at 10 × *Pf* 3D7 EC_{50} without a lag phase and a parasite clearance time (PCT99.9) of <24 h (Table 7, Figure 5).

To assess the human kinase selectivity of **INE963 (1)**, the binding affinities to 468 human kinases were measured at high concentration (10 μM) and directly compared with **3**, the ITD lead compound. **INE963 (1)** is significantly more selective (only 10 out of 468 kinase were inhibited at <10% of control)

https://doi.org/10.1021/acs.jmedchem.1c01995
J. Med. Chem. 2022, 65, 3798−3813

Table 7. *In Vitro P. falciparum* Kill Curve Parameters of INE963 (1)

cpd	dose	lag phase (h)	log PRR[a]	PCT 99.9% (h)
INE963 (1)	10 × EC_{50}	0	>8.0	<24
artemisinin	10 × EC_{50}	0	>8.0	<24

[a]Estimation based on the first 24 h of treatment.

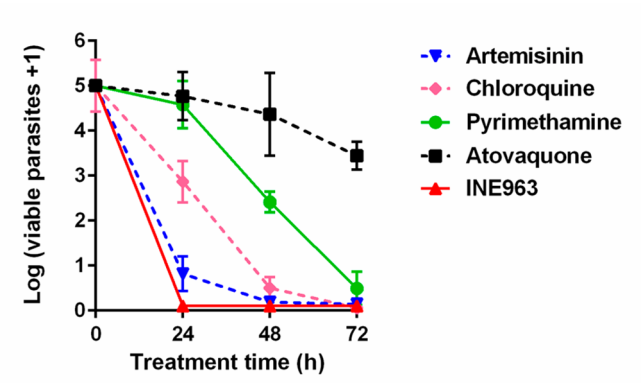

Figure 5. *In vitro P. falciparum* kill kinetics of **INE963 (1)** (PRR assay).

with a S(10) selectivity score of 0.025. This demonstrates an improved human kinase selectivity compared to **3** (which inhibited 53 out of 468 human kinases at <10% of control) with a S(10) selectivity score of 0.132 (Figure 6).[23]

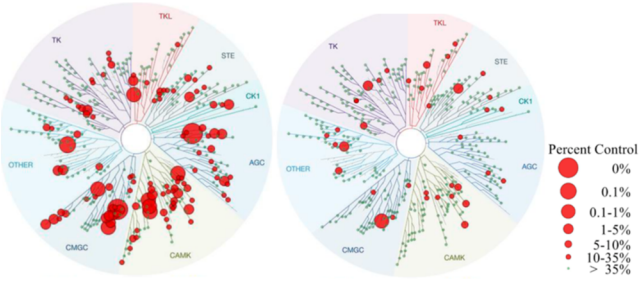

Figure 6. High-concentration (10 μM) human kinase screen of **3** (left) and **INE963 (1)** (right).

Additionally, the IC_{50}'s of **INE963 (1)** on Haspin, FLT3, PIK3CA, and PIM1 were measured in a dose response to be 5.51, 3.60, >50.0, and >50.0 μM, respectively, which illustrates a 600−8333-fold selectivity for *Plasmodium* in cell culture. Compared to compound **3** and earlier imidazothiadiazoles from the patent literatures,[17,18] these data suggest **INE963 (1)** has been substantially optimized for potency on *Plasmodium* while expressly mitigating binding to human kinases.

***In Vivo* Efficacy of INE963 (1).** Based on the potent *in vitro* activity, promising physicochemical properties, and *in vivo* pharmacokinetics, the frontrunner compounds were profiled *in vivo* (Table 8). Oral therapeutic efficacy was evaluated against erythrocytic asexual stages of *Pf* 3D7 *in vivo* in a humanized severe combined immunodeficient (SCID) mouse model measuring the effect on blood parasitemia by flow cytometry and microscopic analysis.[24] Efficacy was assessed following oral administration of the compounds either as four doses or as one single oral dose, and the effect on blood parasitemia was measured up to 60 days post-treatment.

Table 8. *In Vivo* Efficacy of ITD Lead Compounds in *Pf* 3D7 Humanized SCID Mouse Malaria Model[a]

parameter	55	60	65	INE963 (1)
dose[b]	4 x 30	4 x 30	4 x 30	4 x 30
activity[c]	>99.9	>99.9	>99.9	>99.9
DoR[d]	-	>60	>60	>60
C_{max}[e]	1.2	0.59	1.2	0.59
$AUC_{0\text{-}23h}$[f]	15.5	4.5	8.5	5.1
$AUC_{0\text{-}47h}$[g]	-	-	-	-
	3		**INE963 (1)**	
dose[b]	1 x 5	1 x 50	1 x 3	1 x 10
activity[c]	79.4	>99.9	10.5	83.1
DoR[d]	0	>60	0	4.4
C_{max}[e]	0.46	3.5	0.08	0.16
$AUC_{0\text{-}23h}$[f]	6.2	57.3	0.68	1.8
$AUC_{0\text{-}47h}$[g]	8.4	87.1	0.77	2.3
	INE963 (1)			
dose[b]	1 x 15	1 x 20	1 x 30	1 x 100
activity[c]	>99.9	>99.9	>99.9	>99.9
DoR[d]	13.8	16.8	>60	>60
C_{max}[e]	0.16	0.40	0.60	1.5
$AUC_{0\text{-}23h}$[f]	1.3	3.5	6.9	16.7
$AUC_{0\text{-}47h}$[g]	1.7	4.5	8.2	29.8

[a]Data from multiple experiments; n = 1 for four dose groups; n = 2 for compound **3**; n = 1 for 3, 10, 30, and 100 mg/kg of INE963 (**1**); n = 3 for 15 and 20 mg/kg of INE963 (**1**). Average values are showed wherever there is more than one animal. [b]Dose in mg/kg. [c]Activity = Parasitemia reduction compared to untreated controls, in %. [d]DoR = Day of recrudescence, in day. [e]Cmax = Maximum concentration, in μg/mL. [f]AUC0-23 h = Area under the curve from time 0−23 h postdose, in μg*h/mL. [g]AUC0-47 h = Area under the curve from time 0−47 h postdose, in μg*h/mL.

Following four oral doses at 30 mg/kg, the frontrunner compounds tested showed significant parasitemia reduction (>99.9%) at day 5 compared to untreated control mice. In addition, the animals did not show any signs of recrudescence of parasite at day 60 post-treatment, indicating complete cure at these doses. Following on these promising results, **INE963 (1)** was further evaluated in single oral doses. In mice treated with a single oral dose of 15 mg/kg and above, **INE963 (1)** showed >99.9% parasitemia reduction at day 5 postdosing compared to untreated control mice. The effect of a single oral dose was rapidly cidal and reached maximum killing at 15 mg/kg. The effective dose to reduce 90% parasitemia (ED_{90}) was determined to be 11.7 mg/kg. However, with a single dose of 3 mg/kg, 10 mg/kg, 15 mg/kg and 20 mg/kg p.o., mice showed recrudescence of parasites on day 0, day 5, day 14, and day 17, respectively, whereas with a single dose of 30 and 100 mg/kg p.o., mice did not show any signs of recrudescence of parasites at day 60 post-treatment, indicating a complete cure at these doses (Table 8, Figure 7A). Furthermore, dose-related increases in C_{max} and AUC were also observed. The threshold exposure ($AUC_{0-47\ h}$) in this preclinical *Pf* SCID mouse model required for 99.9% parasitemia reduction was 2.1 μg·h/mL (Figure 7B) and for complete cure (>60 days) was 8.2 μg·h/mL (Figure 7C). The results from this study, in conjunction with the predictions of human PK, demonstrate **INE963 (1)** has the potential for single-dose cures of uncomplicated malaria.

https://doi.org/10.1021/acs.jmedchem.1c01995
J. Med. Chem. 2022, 65, 3798−3813

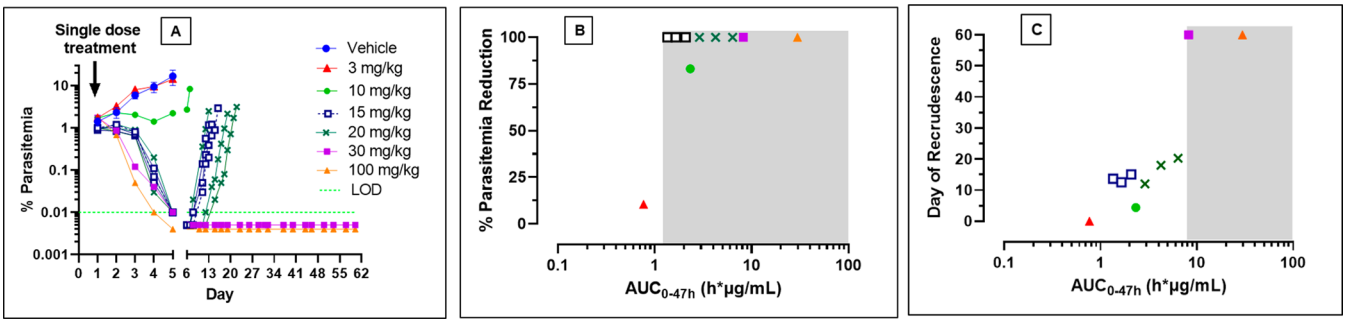

Figure 7. Parasitemia dose−response relationship of **INE963** (**1**) in *Pf* 3D7 humanized SCID mouse model following one single oral dose (A) and the exposure ($AUC_{0-47\ h}$) response relationship with respect to parasitemia reduction (B) and day of recrudescence (C). Data are from multiple experiments with n = 2 for vehicle treatment in each experiment, n = 1 for 3, 10, 30, and 100 mg/kg; n = 3 for 15 and 20 mg/kg dose groups.

Pharmacokinetic Properties of INE963 (1). INE963 (**1**) has high *in vitro* permeability of 9.9×10^{-6} cm/s based on the low efflux Madin Darby canine kidney cell line (MDCK-LE) assay. **INE963** (**1**) is expected to be a P-gp or multidrug resistance 1 (MDR1) protein substrate based on an efflux ratio of 11.8 using transfected MDR1-MDCK cells. However, due to high permeability, this did not significantly impact oral bioavailability. The free-base **INE963** (**1**) is highly crystalline as observed by X-ray powder diffraction (XRPD), and while this form has very low solubility in water (0.0002 mg/mL), there is a dramatic increase of the solubility in SGF and FaSSIF (>2.0 and 1.3 mg/mL) which likely has a positive impact on oral absorption. Overall, **INE963** (**1**) is a lipophilic base, $\log D_{pH7.4}$ = 3.1 and pK_a = 8.7, with high solubility and is classified as a BCS class III drug. **INE963** (**1**) displays minimal inhibition of CYP450s, with measured IC_{50}'s ranging from 4.5 to 8.5 μM for 2C9, 2C19, 2B6, and 2C8; with all others >20 μM. Across the species tested, plasma protein binding is >99% with low *in vitro* microsomal and hepatocyte clearance (CL_{int}). In addition, **INE963** (**1**) exhibits high membrane and tissue binding *in vivo* (i.e., high volume) which minimizes the amount of free drug exposed to hepatic clearance and thus increases the apparent *in vivo* $T_{1/2}$ (Table 9).

In vivo pharmacokinetics of **INE963** (**1**) have been studied in mice, rats, and dogs where the absorption was moderate to slow (T_{max} 4−24 h) with good bioavailability (%*F*) of 39−74% across the species. **INE963** (**1**) has a low blood clearance (<10% of hepatic blood flow in rat and mouse and <20% of hepatic blood flow in dog) and a high volume of distribution, resulting in long half-lives (15−24 h) across the species (Table 9).

***In Vitro* Metabolism of INE963 (1).** The *in vitro* metabolism of **INE963** (**1**) was first investigated following incubation in rat, dog, and human cryopreserved hepatocytes at 10 μM for up to 4 h, resulting in two metabolites: hydroxylation on the isopropyl moiety (<2.5%) with subsequent dehydration (<1.5%). Neither uptake issues (MDCK-LE permeability = 9.9×10^{-6} cm/s) nor saturation of metabolic enzymes were responsible for the low metabolic turnover of **INE963** (**1**), as high metabolic stability was also observed in human liver microsomes at 0.5 and 6 μM. Long-term *in vitro* incubations may increase metabolite formation for low turnover compounds.[25,26] Subsequently, **INE963** (**1**) was incubated for up to 168 h in rat, dog, and human primary hepatocyte/nonparenchymal stromal cell cocultures (at 10 μM). A summary of the *in vitro* metabolites obtained from this study is provided in Figure 8. Hydroxylation and demethylation represented the main phase I metabolic pathways, whereas acetylation (rat and human) and formylation (mainly in dog) seemed to be the main phase II metabolic pathways *in vitro*. Regardless of the species, hydroxylated **INE963** (M13) was the most intense *in vitro* metabolite based on mass spectrometric responses. Moreover, all *in vitro* metabolites

Table 9. Summary of Physiochemical and Pharmacokinetic Properties of INE963 (1)

assay	**INE963** (**1**) data
physical form by XRPD	free base; highly crystalline
pK_a	4.0, 8.7
$\log D_{7.4}$	3.1
solubility in water (mg/mL)	0.0002
solubility in FaSSIF pH 6.5 (mg/mL)	1.3
solubility SGF pH 2.0 (mg/mL)	>2
permeability (MDCK-LE; Papp AB × 10^6 cm/s)	9.9
CYP inhibition (2C9, 2C19, 2B6, 2C8, all others >20 μM)	4.5, 5.4, 6.0, 8.5
efflux ratio (MDR1-MDCK; BA/AB)	11.8
biopharmaceutical class (BCS class)	III (up to 1000 mg dose)
mouse, rat, dog, human PPB (% bound)	>99, >99, >99, >99
mouse, rat, dog, human microsome CL_{int} (μL/min/mg)	<25, 29, <25, 25.4
rat, dog, human hepatocyte CL_{int} (μL/min/10^6 cells)	7.1, <4, <4
mouse, rat, dog *in vivo* CL (mL/min/kg)[a]	4.0, 5.9, 5.4
mouse, rat, dog *in vivo* V_{ss} (L/kg)[a]	7.0, 8.3, 6.3
mouse, rat, dog *in vivo* half-life $T_{1/2}$ (h)[a]	22.5, 20.4, 15.1
mouse, rat, dog *in vivo* oral bioavailability (%*F*)[a]	47, 39, 74

[a]*In vivo* PK data from a crystalline formate-salt batch of **INE963** (**1**), using blood concentration.

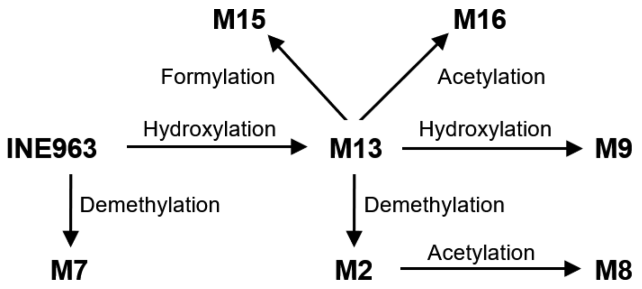

Figure 8. *In vitro* metabolism of **INE963** (**1**) following incubation in rat, dog, and human primary hepatocyte/nonparenchymal stromal cell cocultures at 10 μM for up to 168 h.

https://doi.org/10.1021/acs.jmedchem.1c01995
J. Med. Chem. 2022, 65, 3798−3813

Table 10. Summary of Predicted Human Pharmacokinetic Parameters for INE963 (1)

PK parameter	predicted human value	units	notes
clearance (CL)	1.6	mL/min/kg	based on allometric scaling method with brain weight correction
volume steady state (V_{ss})	7.2	L/kg	mean values from allometric scaling using single species (mouse, rat, dog)
apparent $T_{1/2}$	~60	hours	fit to 3-compartmental model with linear elimination after IV dose (GastroPlus)
bioavailability (F)	~70	%	a gut PBPK model with an ACAT model after an oral dose at 1 mg/kg in IR tablet (Fed) (GastroPlus)

formed in human hepatocytes were also obtained following incubation in rat or dog hepatocytes. Current investigations are ongoing to further assess the metabolism of **INE963** (**1**) *in vivo*, which will be published at later stage.

Human Pharmacokinetic Prediction of INE963 (1). Due to the low or no hepatic turnover *in vitro*, either liver microsomal or hepatocyte assays under-predicted the *in vivo* clearance observed in preclinical species. For this reason, a direct *in vitro in vivo* extrapolation could not be established. Allometry-based approaches using *in vivo* PK data from mice, rats, and dogs were utilized to predict human clearance (CL) and steady-state volume (V_{ss}). Since no human-specific metabolites have been observed from *in vitro* studies and **INE963** (**1**) has low CL and high V_{ss} across all species *in vivo*, the overall confidence in using allometry methods is good. Using all three species data, clearance and steady-state volume of distribution in humans were estimated as 1.6 mL/min/kg, and 7.2 L/kg, respectively. From these parameters, the Wajima method was used to generate a predicted human IV time−concentration plot, and further a gut ACAT model was used for the prediction of a human oral PK profile. The predicted human PK parameters are summarized in Table 10. The bioavailability is estimated to be ~70% after a single oral dose as an immediate release (IR) tablet under fed conditions, and the apparent $T_{1/2}$ is predicted to be long (~60 h). Overall, the forecasted PK profile is supportive of an oral single-dose curative therapy in patients. Based on emerging PK data from the first-in-human study, modeling is in progress to identify single doses sufficient to maintain efficacious concentrations (estimated to be from 35 to 150 nM based on the SCID mouse model) for multiple Plasmodium blood-stage life cycles (4−6 days).

CONCLUSION

In summary, **INE963** (**1**) offers several advantageous properties as an antimalarial candidate for single-dose cure therapy of uncomplicated malaria, including moderate-to-high bioavailability with a projected human half-life of ~60 h. In the humanized SCID mouse *Pf* malaria model, **INE963** (**1**) achieved 99.9% parasite reduction in blood with a single oral dose of 15 mg/kg and a >60 days full cure with a single oral dose of 30 mg/kg. Furthermore, **INE963** (**1**) shows high potency on resistant strains and field isolates, a high barrier to resistance *in vitro*, a fast-acting phenotype in *Plasmodium* assays, and a MoA that is unknown but likely to be novel. **INE963** (**1**) also has a high degree of selectivity (>1000-fold) against comprehensive *in vitro* safety panels, including human kinases that have previously been reported as sensitive to 5-aryl-2-amino-ITDs. Additionally, **INE963** (**1**) was evaluated in off-target safety panels, GLP safety pharmacology, genetic toxicity, and 2-week GLP toxicity studies in rats and dogs and was determined to have an adequate safety profile for advancement into clinical studies. Taken together, the balance of these properties position **INE963** (**1**) as a unique antimalarial clinical candidate with a high barrier to resistance and the potential for single-dose cures. Ph1 clinical studies are currently underway in healthy volunteers.

SYNTHESIS

The gram-scale synthesis of **INE963** (**1**) outlined in Scheme 1 commenced with bromination of 1,3,4-thiadiazol-2-amine (**68**), which

Scheme 1. Synthesis of INE963 (1)[a]

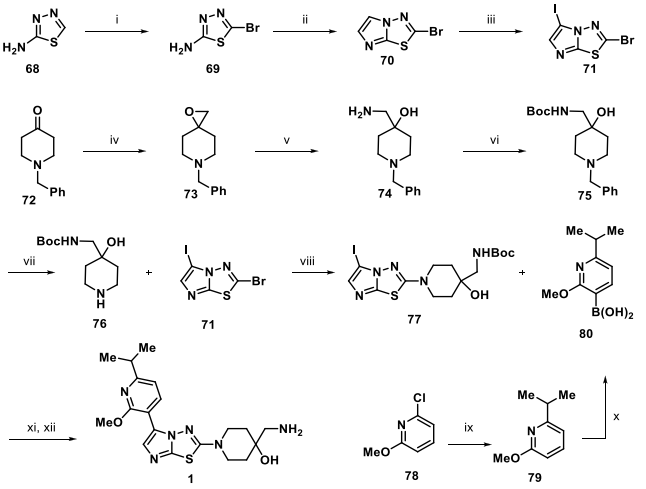

[a]Reagents and conditions: (i) Br_2, $NaHCO_3$, MeOH, 0 °C, 64%; (ii) 2-chloroacetaldehyde, H_2O, EtOH, reflux, 48 h, 20%; (iii) NIS, DMF, RT, 37%; (iv) ^{t}BuOK, DMSO, trimethylsulfoxonium iodide, RT, then benzylpiperidin-4-one, 94%; (v) aq. NH_3, 5 °C then RT, 83%; (vi) Boc_2O, Et_3N, 2-Me THF, 0 °C to RT, 62%; (vii) H_2, Pd/C, MeOH, 60 °C, 70%; (viii) **76**, **71**, DIPEA, 2-MeTHF, 85 °C, 52%; (ix) $Fe(acac)_3$, NMP, THF, −50 °C, isopropyl magnesium chloride, 90%; (x) *n*-BuLi, TMEDA, tri-isopropyl borate, −78 °C to RT, 87%; (xi) **77**, **80**, $PdCl_2$(dppf)-DCM, aq. K_3PO_4, 1,4-dioxane, 90 °C, 70%; (xii) formic acid, 0 °C to rt then NaOH, RT, 72%.

then underwent cyclization with 2-chloroacetaldehyde, followed by iodination to furnish key intermediate 2-bromo-5-iodo-imidazothiadiazole (**71**). The Corey−Chaykovsky reaction of 1-benzylpiperidin-4-one (**72**) provided the epoxide **73** in high yield, which was subsequently opened up with ammonia before Boc-protection to yield **75**. Removal of the benzyl group furnished intermediate **76** which underwent an SnAr reaction with the bromide of key intermediate **71** to yield 77. The boronic ester **80** was prepared in two high yielding steps starting with an iron-catalyzed addition of isopropyl Grignard reagent to 2-chloro-6-methoxypyridine (**78**), followed by treatment with *n*-butyllithium and subsequent reaction with tri-isopropyl borate to yield **80**. Suzuki coupling of **80** with 77, followed by Boc group removal with formic acid, then provided **INE963** (**1**).

Since the route described in Scheme 1 offered substantial flexibility and was amenable to gram-scale synthesis of **INE963** (**1**), we implemented a general synthetic approach shown in Scheme 2

https://doi.org/10.1021/acs.jmedchem.1c01995
J. Med. Chem. 2022, 65, 3798−3813

Scheme 2. General Pathway to Synthesize Imidazothiadiazole Analogs[a]

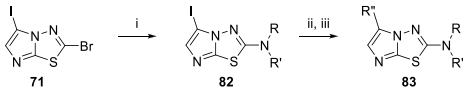

[a]Reagents and conditions: (i) RR′NH, DIPEA, CH_3CN or NMP or DMSO, 90−110 °C; (ii) R″-boronic acid/ester, $PdCl_2$(dppf)-DCM (5 mol %), aq. K_3PO_4, 1,4-dioxane, 80−90 °C; (iii) HCl or HCOOH or TFA, 0 °C to RT.

starting with the key intermediate ITD **71**. A facile SnAr reaction with a variety of primary and secondary amines furnished the 2-amino-substituted imidazothiadiazole **82** in a moderate to high yield. Subsequently, cross-coupling with a range of different boronic acids/esters using palladium catalysis followed by Boc deprotection gave the target compounds **83**.

EXPERIMENTAL SECTION

General Procedures. All materials and reagents used were of the best commercially available grade and used without further purification. Normal-phase column chromatography was carried out using prepacked silica gel cartridges on a Combiflash Rf separation system by Teledyne ISCO. ^{1}H NMR spectra were determined on a Varian 400 or Bruker 300 or 400 and 500 MHz NMR spectrometers. The following abbreviations are used: s = singlet, d = doublet, dd = doublet of doublets, t = triplet, q = quartet, m = multiplet, bs = broad singlet. Preparative HPLC was performed on a Waters Prep HPLC system using a C18 reversed-phase column eluting with gradient mixtures of water/acetonitrile containing a modifier 0.05% trifluoroacetic acid. All compounds >95% purity by HPLC analysis. The purity of the final compounds was confirmed by UPLC-MS and UPLC. Additionally, all final compounds presented with *in vivo* data have been confirmed by ^{1}H NMR, LCMS, and HRMS in the Supporting Information. The human biological samples were sourced ethically, and their research use was in accord with the terms of the informed consents under an IRB/EC approved protocol. All animal studies were ethically reviewed and carried out in accordance with European Directive 2010/63/EEC and the GSK Policy on the Care, Welfare, and Treatment of Animals. Human erythrocytes for *in vivo* studies were obtained from the Basque Center of Transfusion and Human Tissues, Galdakao, Spain; the Centro de Transfusiones de la Comunidad de Castilla y León, Valladolid, Spain; and the Bank of Blood and Tissues, Barcelona, Spain. Clinical isolate assays in Brazil and Uganda were performed as previously described.[19,20]

*5-Bromo-1,3,4-thiadiazol-2-amine (**69**).* To 1,3,4-thiadiazol-2-amine (**68**) (500 g, 4.95 mol) in MeOH (5 L), $NaHCO_3$ (830.9 g, 9.89 mol) was added at room temperature (RT). The mixture was cooled to 0−5 °C, and bromine (792.0 g, 4.95 mol) was added dropwise over a period of 1 h. The mixture was warmed to RT and stirred for 3 h, and the solid was filtered and washed with MeOH (500 mL). The solid was slurried in water (10 L) for 1 h and collected and washed with water (1 L). The solid was slurried in MeOH (1.5 L), filtered, and washed with MTBE (1 L) to give the title compound (554.0 g, 64%) as yellowish solid. ^{1}H NMR (400 MHz, DMSO-d_6): δ ppm 7.51 (brs, 2H). ESI MS (m/z): $[M + H]^+$ calcd for $C_2H_3BrN_3S$ 179.9, found 179.9.

*2-Bromoimidazo[2,1-b][1,3,4]thiadiazole (**70**).* To a mixture of 5-bromo-1,3,4-thiadiazol-2-amine (**69**) (500.0 g, 2.78 mol) in water and EtOH (1:1; 5 L) was added a 44% aqueous solution of 2-chloroacetaldehyde (1425.9 g, 7.78 mol) over a period of 15 min at RT. The reaction mixture was heated at reflux over a period of 1 h and stirred for 48 h. After completion of the reaction, the reaction mixture was quenched with 8% aqueous solution of sodium bicarbonate (5 L), and EtOAc (10 L) was added to it. The mixture was stirred for 10 min at RT. The reaction mixture was filtered through Celite bed, and bed was washed with EtOAc (1.0 L). The organic layer was separated, and an aq. layer was extracted with EtOAc (1.0 L × 2). The combined organic layer was concentrated and purified on silica gel (100−200 mesh, EtOAc in heptane from 16.7% to 25%) to give the title compound (88.5 g, 20%) as yellowish solid. ^{1}H NMR (300 MHz, DMSO-d_6): δ ppm 8.22 (d, J = 1.2 Hz, 1H), 7.39 (d, J = 0.8 Hz, 1H). ESI MS (m/z): $[M + H]^+$ calcd for $C_4H_3BrN_3S$ 203.9, found 203.9.

*2-Bromo-5-iodoimidazo[2,1-b][1,3,4]thiadiazole (**71**).* To 2-bromoimidazo[2,1-*b*][1,3,4]thiadiazole (**70**) (50.0 g, 245 mmol) in DMF (500 mL), NIS (66.1 g, 294 mmol) was added at RT on portion, and the resulting mixture was stirred for 2.5 h. Another NIS (11.0 g, 49 mmol) was added and stirred for another 1.5 h. The reaction mixture was diluted with EtOAc (2.0 L), and then the reaction mixture was washed with aqueous $Na_2S_2O_3$ solution (500 mL). The organic layer was washed with ice cooled water (3 × 250 mL) and further washed with brine (250 mL), dried over anhydrous Na_2SO_4, filtered, and concentrated. The residue was slurried in MeCN (100 mL) for 30 min, and the solid was filtered and washed with MeCN (50 mL) to give the title compound (40.4 g, 37%) as white solid. ^{1}H NMR (400 MHz, DMSO-d_6): δ ppm 7.43 (s, 1H). ESI MS (m/z): $[M + H]^+$ calcd for $C_4H_2BrIN_3S$ 329.8, found 329.7.

*6-Benzyl-1-oxa-6-azaspiro[2.5]octane (**73**).* ^{t}BuOK (177.9 g, 1.59 mol) was added in portions to DMSO (2.0 L) at RT under N_2, then trimethylsulfoxonium iodide (319.8 g, 1.45 mol) was added in portion slowly over 15 min at RT. The resulting solution was stirred at RT for 1 h. A solution of 1-benzylpiperidin-4-one (**72**) (250 g, 1.32 mol) in DMSO (0.5 L) was added at RT over 30−40 min. The reaction was stirred at RT for 1 h, then the solution was quenched with water (2.5 L) and extracted with MTBE (2.5 L × 2). The combined organic layers were washed with brine (2.5 L), dried over Na_2SO_4, filtered, and concentrated to give the title compound (253 g, 94%) as yellowish liquid. ^{1}H NMR (400 MHz, DMSO-d_6): δ ppm 7.26−7.38 (m, 5H), 3.59 (s, 2H), 2.55−2.67 (m, 5H), 1.82−1.89 (m, 2H), 1.57−1.60 (m, 2H). ESI MS (m/z): $[M + H]^+$ calcd for $C_{13}H_{18}N$ 204.1, found 204.1.

*4-(Aminomethyl)-1-benzylpiperidin-4-ol (**74**).* To 6-benzyl-1-oxa-6-azaspiro[2.5]octane (**73**) (250 g, 1.23 mol) in MeOH (1.5 L), aqueous ammonia (3 L, 4.15 mol) was added dropwise at 5−10 °C over 15 min. The resulting mixture was stirred at RT for 16 h and diluted in DCM (3.5 L). The aqueous layer was separated and extracted with DCM (3 L × 3). The combined organic layers were washed with NaOH (1 *N*, 3 L) and brine (3 L), dried on Na_2SO_4, and concentrated to give the title compound (225 g, 83%) as off-white solid, which was used for next step without further purification.

*tert-Butyl ((1-Benzyl-4-hydroxypiperidin-4-yl)methyl)carbamate (**75**).* 4-(Aminomethyl)-1-benzylpiperidin-4-ol (**74**) (430 g, 1.95 mol) was suspended in 2-Me THF (8.6 L), and Et_3N (197.5 g, 1.95 mol) was added before the reaction was cooled to 0 °C. Then a solution of Boc_2O (511.5 g, 2.34 mol) in 2-Me THF (400 mL) was added dropwise at 0 °C over 20 min. The resulting solution was stirred for 16 h, and the mixture was quenched with water (2 L) and brine (2 L). The organic layer was washed with brine (2 × 2 L), dried over Na_2SO_4, filtered, concentrated, and purified by silica gel (60−120 mesh) using an initial elution with 50−80% EtOAc in hexanes then 5−20% MeOH in DCM to give the title compound (396 g, 62%) as off-white solid. ^{1}H NMR (400 MHz, $CDCl_3$): δ ppm 7.24−7.32 (brs, 5H), 4.90 (s, 1H), 3.53 (s, 2H), 3.15 (d, J = 6.0 Hz, 2H), 2.59−2.62 (m, 2H), 2.30−2.40 (m, 3H), 1.56−1.67 (m, 4H), 1.44 (s, 9H). ESI MS (m/z): $[M + H]^+$ calcd for $C_{18}H_{29}N_2O_3$ 321.2, found 321.2.

*tert-Butyl ((4-Hydroxypiperidin-4-yl)methyl)carbamate (**76**).* *tert*-Butyl ((1-benzyl-4-hydroxypiperidin-4-yl)methyl)carbamate (**75**) (363.0 g, 1.13 mol) was dissolved in MeOH (2.5 mL) before Pd/C (90.75 g, 20%) was added under N_2. The resulting mixture was evacuated with hydrogen gas and given 15 kg/cm^2 of pressure. The mixture was stirred for 16 h at 60 °C, then was filtered through a Celite bed, washed with MeOH (2 L), and concentrated. The crude product was slurried in IPA (700 mL), filtered, and washed with IPA (200 mL) to give the title compound (180 g, 70%) as white solid. ^{1}H NMR (400 MHz, $CDCl_3$): δ ppm 4.95 (brs, 1H), 3.13−3.21 (d, J = 6.0 Hz, 2H), 2.91−2.97 (m, 2H), 2.82−2.87 (m, 2H), 2.08 (brs, 2H), 1.47−1.54 (m, 4H), 1.43 (s, 9H). ESI MS (m/z): $[M + H]^+$ calcd for $C_{11}H_{23}N_2O_3$ 231.2, found 231.1.

https://doi.org/10.1021/acs.jmedchem.1c01995
J. Med. Chem. 2022, 65, 3798−3813

*tert-Butyl ((4-Hydroxy-1-(5-iodoimidazo[2,1-b][1,3,4]thiadiazol-2-yl)piperidin-4-yl)methyl)carbamate (**77**).* A mixture of *tert*-butyl ((4-hydroxypiperidin-4-yl)methyl)carbamate (**76**) (155 g, 076 mol), 2-bromo-5-iodoimidazo[2,1-*b*][1,3,4]thiadiazole (233.2 g, 0.71 mol), and DIPEA (174.0 g, 1.35 mol) in 2-MeTHF 1.55 L, 10 V) was heated to 85 °C for 9 h. The reaction was stirred in water (10 V) at RT for 15 min before the layers were separated. The aqueous layer was extracted twice with EtOAc (2 × 10 V). The combined organic layers were washed with brine, dried over Na_2SO_4, filtered, concentrated, and triturated in DCM (5 V) for 1 h at RT. The suspension was filtered, washed with DCM (1 V), and dried under vacuum to give the title compound (168 g, 52%) as light brown solid. ^{1}H NMR (400 MHz, MeOD-d_4): δ ppm 7.06 (s, 1H), 2.69−3.72 (m, 2H), 3.45−3.52 (m, 2H), 3.11 (s, 2H), 1.63−1.76 (m, 4H), 1.44 (s, 9H). ESI MS (m/z): $[M + H]^+$ calcd for $C_{15}H_{22}IN_5O_3S$ 480.1, found 480.0.

*2-Isopropyl-6-methoxypyridine (**79**).* To a solution of 2-chloro-6-methoxypyridine (**78**) (90 g, 0.63 mol) in THF (810 mL) and NMP (90 mL) was added $Fe(acac)_3$ (2.21 g, 1 mol %) at RT. The reaction mixture was purged with N_2 for 30 min at RT and then cooled to −50 °C before slow addition of a solution of isopropyl magnesium chloride in THF (96.71 g, 1.5 equiv) over 1.5 h. The reaction mixture was stirred for 30 min. The reaction mixture was quenched with water (2 equiv) slowly at −40 °C, then warmed to 0 °C, followed by the addition of 1.5 N HCl (90 mL) at 0−5 °C (highly exothermic) and further diluted with water (800 mL). The mixture was diluted with MTBE (900 mL). The organic layer was separated and washed with water (5 × 900 mL), dried over Na_2SO_4, distilled under vacuum at 40 °C, and further dried under high vacuum for 2 h at 40 °C to give the title compound (86 g, 90%). ^{1}H NMR (400 MHz, $CDCl_3$): δ ppm 7.48−7.46 (m, 1H), 6.72−6.70 (d, J = 8 Hz, 1H), 6.53−6.51 (m, 1H), 3.92 (m, 3H), 3.02−2.90 (m, 1H), 1.28−1.26 (m, 6H). ESI MS (m/z): $[M + H]^+$ calcd for $C_9H_{14}NO$ 152.1, found 152.1.

*(6-Isopropyl-2-methoxypyridin-3-yl)boronic Acid (**80**).* To a solution of 2-isopropyl-6-methoxypyridine (**79**) (100 g, 0.66 mol) in THF (810 mL) was added TMEDA (80.7 g, 0.69 mol) at RT under N_2 atmosphere. The resulting mixture was cooled to −78 °C, and slowly *n*-BuLi (2.5 M in hexane, 63.48 g, 0.99 mol) was added. The reaction was allowed to reach RT and was stirred for 1 h at RT. Further, the reaction was cooled to −78 °C, and then tri-isopropyl borate (286.1 g, 1.52 mol) was slowly added. The reaction was warmed to RT and was stirred for 3 h at RT. After completion, the reaction was cooled to 0 °C, quenched with 1.5 N HCl (400 mL) at 0 °C, and further diluted with water (400 mL). The aqueous layer was extracted with EtOAc (400 mL). The organic layer was washed twice with brine (800 mL), dried over Na_2SO_4, distilled under vacuum at 30 °C, and purified on silica gel (EtOAc/Hexane) to give the title compound (123 g, 95%). ^{1}H NMR (400 MHz, $CDCl_3$): δ ppm 8.05−7.99 (m, 1H), 6.91−6.78 (m, 1H), 6.03 (s, 1H), 4.07−4.03 (m, 3H), 3.00−2.93 (m, 1H), 1.35−1.22 (m, 6H).

*tert-Butyl ((4-Hydroxy-1-(5-(6-isopropyl-2- methoxypyridin-3-yl)-imidazo[2,1-b][1,3,4]thiadiazol-2-yl)piperidin-4-yl)methyl)-carbamate (**81**).* To a solution of (6-isopropyl-2-methoxypyridin-3-yl)boronic acid (**80**) (170 g, 0.35 mol) and *tert*-butyl ((4-hydroxy-1-(5-iodoimidazo[2,1-*b*][1,3,4]thiadiazol-2-yl)piperidin-4-yl)methyl)-carbamate (**77**) (76.08 g, 0.39 mol) in 1,4-dioxane (1.7 L) under N_2 atmosphere was added a prepared solution of K_3PO_4 (225.85 g, 1.064 mol) in water (340 mL). The reaction mixture was purged under N_2 gas for 15 min before $Pd(dppf)Cl_2$.DCM (20.27 g, 0.025 mol) was added. The reaction mixture was heated to 85 °C for 16 h. The reaction was treated with water (3.4 L) for 30 min at RT and then at 10 °C for 1 h. The resulting solids were washed with water (850 mL), dried under vacuum, and further washed with MTBE (1.5 mL). The isolated solid was purified on silica gel (2−3% MeOH/DCM), followed by MTBE slurry of the major fraction, resulting in an off-white solid. The product was dissolved in DCM (3.4 L) and heated to 40 °C. The resulting solution was treated with siliabond thiol (30 wt %) at 40 °C for 6 h before it was filtered through Celite bed at 30 °C and washed with DCM (340 mL). The filtrate was resubjected to siliabond thiol (30 wt %) treatment at 40 °C for 6 h, filtered through Celite at 30 °C, and washed with DCM (340 mL). The filtrate was evaporated under reduced pressure followed by codistillation with MTBE (2 × 850 mL) and slurried in MTBE (850 mL) for 1 h at 30 °C. The solids were filtered, washed, and dried further to give the title compound (123 g, 70%) as a white solid. ^{1}H NMR (400 MHz, $CDCl_3$): δ ppm 8.50 (d, J = 7.6 Hz, 1 H), 7.68 (s, 1 H), 6.83 (d, J = 7.6 Hz, 1 H), 5.02 (bs, 1 H), 4.06 (s, 3 H), 3.71−3.69 (m, 2H), 3.56−3.49 (m, 2H), 3.18 (d, J = 6.4 Hz, 2 H), 2.96 (quintet, J = 6.8 Hz, 1 H), 1.78−1.61 (m, 6H), 1.45 (s, 9H), 1.25 (m, 6H). ESI MS (m/z): $[M + H]^+$ calcd for $C_{24}H_{35}N_6O_4S$ 503.2, found 503.3.

*4-(Aminomethyl)-1-(5-(6-isopropyl-2-methoxypyridin-3-yl)-imidazo[2,1-b][1,3,4]thiadiazol-2-yl)piperidin-4-ol (**INE963**; **1**).* *tert*-Butyl ((4-hydroxy-1-(5-(6-isopropyl-2-methoxypyridin-3-yl)imidazo-[2,1-*b*][1,3,4]thiadiazol-2-yl)piperidin-4-yl)methyl)carbamate (**81**) (50 g, 0.099 mol) was collected to 0 °C before formic acid (80 mL, 9.95 mol) was slowly added under N_2 atmosphere. The reaction mixture was allowed to warm to RT and continue to stir for 7 h at RT. The excess of formic acid was evaporated under reduced pressure at 30 °C and then codistilled with MeCN (5 × 360 mL). The resulting solids were slurried in MeCN (3.6 L) and stirred for 1 h at RT and then at 10 °C for 1 h. The solids were washed with MeCN (150 mL) and then dried to obtain 37 g of formate salt. Combined with another similar batch size, the formate salt (72 g) was dissolved in water (580 mL), and a solution of NaOH (20% in Water, 72 mL) was added to adjust the pH to 13. The mixture was stirred for 1 h at RT. The solids were filtered and washed with water (360 mL), then washed with MTBE (360 mL), and finally dried under vacuum for 16 h. The solids were taken again in water (720 mL) and stirred for 2 h at RT. The solids were filtered, washed with water (360 mL), washed with MTBE (360 mL), and then dried under vacuum at 45 °C for 48 h to give the title compound (62 g, 72%). ^{1}H NMR (300 MHz, DMSO-d_6) δ 8.55 (d, J = 7.7 Hz, 1H), 7.56 (s, 1H), 7.00 (d, J = 7.8 Hz, 1H), 4.42 (s, 1H), 4.00 (s, 3H), 3.65 (dd, J = 10.4, 6.5 Hz, 2H), 3.8−3.41 (m, 2H), 3.33 (s, 2H), 2.97 (h, J = 6.8 Hz, 1H), 1.63−1.56 (m, 4H), 1.26 (d, J = 6.9 Hz, 6H). ESI HRMS $[M + H]^+$ for $C_{19}H_{27}N_6O_2S$ calcd 403.1911, found 403.1907. LCMS R_t: 2.65 min; purity: >99%.

***Pf* 3D7 Phenotypic Assay.** Following an established *Pf* protocol,[27] parasite cultures were grown in media (RPMI 1640 medium (10.4 g/L) with 0.5% Albumax II, 200 μM hypoxanthine, 50 mg/L gentamicin sulfate, 35 mM Hepes, 2.0 g/L sodium bicarbonate, and 11 mM glucose) and human erythrocytes. Cultures were maintained at 37 °C in an incubator with 5% CO_2. *In vitro* antiplasmodium activity was measured according to a modified SYBR Green cell proliferation assay.[28] Dose−response curve data were normalized based on fluorescence signal values from DMSO treated wells (0% inhibition) and mefloquine treated wells (100% inhibition) at a final concentration of 10 μM. The standard logistic regression model was applied for curve fitting in order to determine the EC_{50}.[29]

HepG2 Cytotox Assay. HepG2 are adherent cells that were maintained in Dulbecco's modified Eagle's medium-F12 supplemented with 1% penicillin/streptomycin and 10% heat-inactivated FBS. Fifty μL of a 5 × 10^4 cells/mL suspension were dispensed in white, solid 384-well plates (Greiner). Cells were exposed to compounds for 72 h, after which cell viability was quantified by using CellTiter-Glo. This reagent measures ATP release based on the mono-oxygenation of luciferin catalyzed by Mg^{2+}, ATP, and molecular oxygen. EC_{50} values were calculated from two independent experiments performed in triplicate using the Graphpad Prism software. The standard logistic regression model was applied for curve fitting in order to determine the EC_{50}.[29]

Haspin Kinase assay. The assay was done in assay buffer consisting of 50 mM 4-(2-hydroxyethyl)-1-piperazine ethanesulfonic acid or HEPES at pH 7.5, 5 mM $MgCl_2$, 0.01% Tween-20, 0.1% glycerol, 0.5 mM (tris(2-carboxyethyl)phosphine) or TCEP, and 0.01% bovine serum albumin. All reaction was performed at RT. Compounds were prespotted and incubated with 10 mL of assay buffer containing 0.05 pM of human Haspin kinase domain for 30 min. The reaction was initiated by adding 10 mL of assay buffer containing 0.3 nM H3 biotin peptide and 30 mM of ATP for 90 min. The assay was stopped with 100 mM EDTA. The luminescence signal

https://doi.org/10.1021/acs.jmedchem.1c01995
J. Med. Chem. 2022, 65, 3798−3813

was detected by adding using 10 mg/mL of streptavidin donor beads and 42 ng/mL of antiphospho-histone H3 (Thr3) antibody together with 10 mg/mL protein A acceptor beads. The plates were briefly spun, sealed, and incubated in the dark overnight before reading them with Envision.

***Pf* 3D7 Phenotypic Resistance Selection Methods.** Three different protocols were used to raise resistance against ITD leads in *Pf* blood stages. Culture conditions were as described. Asexual parasites were exposed to a drug concentration of $3 \times IC_{50}$ at a single inoculum of 10^9 parasites in duplicates. The parasites cleared from the culture within days. The cultures were maintained and monitored for parasites growth on a routine basis. When no parasites recrudesced within 60 days, the cultures were discarded. The experiment was repeated in the presence of 5 μM ethylmethanesulfonate (EMS), a mutagen that increases the chance for resistance development. 10^9 parasites were incubated in duplicate for 2 h with EMS prior to applying the drug pressure to raise resistant parasites. Cultures were again monitored for 60 days before discarding them after no recrudescence was observed. Lastly, we exposed parasites to low doses of drug cycling over a period of 7 months. 10^8 parasites were maintained between 0.5% and 10% parasitemia and exposed to short pulses of drug incubation (1−4 days). After each treatment, the drug was removed, and parasites were allowed to recover. The drug concentration was slowly raised from $0.5 \times$ to $8 \times IC_{50}$, but parasites either failed to recover or did not show a resistant phenotype as measured by 72 h growth inhibition assays. The experiment was run in duplicate and four biological replicates.

***In Vivo* Efficacy Studies using *P. falciparum* SCID Mouse Model.** *In vivo* animal experiments were performed at The Art of Discovery SL. These studies were approved by The Art of Discovery Institutional Animal Care and Use Committee (TAD-IACUC). The committee is certified by the Biscay County Government (Bizkaiko Foru Aldundia, Basque Country, Spain) to evaluate animal research projects from Spanish institutions according to point 43.3 from Royal Decree 53/2013, from the first of February (BOE-A-2013-1337). All experiments are carried out in accordance with European Directive 2010/63/EU.

The compound efficacy was assessed in the murine *P.falciparum* SCID model as described previously. Briefly, 22−28 g female NOD-SCID IL- 2Rγnull mice (NSG) (Charles River, France) previously engrafted with human erythrocytes (>40% of human erythrocytes in peripheral blood) were intravenously infected with *Pf* 3D70087/N9-infected erythrocytes (0.3 mL of 1.17×10^8 parasitized-erythrocytes per mL) 72 h before drug treatment inception. At this point (day 1 of the study), mice had 1−2% of parasitemia on average, and the mice were randomly allocated to selected treatments. Compound was formulated in 0.5% methylcellulose and 0.5% Tween 80 in double distilled water administered by oral gavage at 10 mL/kg dose volume on day 1 of the study either as four oral doses or one single oral dose. The effect of treatment on parasitemia was assessed by measuring the percentage of infected erythrocytes in peripheral blood every 24 h until parasitemia was below the selected limit of quantitation (usually 0.01%) by flow cytometry. The parasitemia in mice was regularly measured up to day 60 of experiment to check the presence of circulating parasitized human erythrocytes. In addition, during the study, samples of peripheral blood were taken between 0 and 71 h postdose from mice to measure the concentration of drugs in blood after oral administration. The drugs were extracted from blood samples by protein precipitation using standard liquid−liquid extraction. Briefly, 10 μL of blood samples were mixed with 60 μL of acetonitrile containing internal standard (100 ng/mL of trimipramine-d_3 in methanol), vortexed, and centrifuged, 60 μL of supernatant was mixed with 55 μL of water. These samples were analyzed by LC-MS/MS for quantification in a Waters Micromass UPLC-TQD (Waters, Manchester, UK) under optimized conditions. Data analysis is performed using Phoenix WinNonlin version 7.0 (Certara) to calculate PK parameters via noncompartmental analysis.

■ ASSOCIATED CONTENT

Supporting Information

The Supporting Information is available free of charge at https://pubs.acs.org/doi/10.1021/acs.jmedchem.1c01995.

Synthetic schemes and experimental procedure of compounds **2**−**67**, X-ray crystallization data for Haspin with compound **5**, and ^{1}H NMR and LC Chromatograms of all in vivo compounds (PDF)

Molecular formula strings CSV (CSV)

■ AUTHOR INFORMATION

Corresponding Authors

Benjamin R. Taft − *Global Discovery Chemistry, Novartis Institutes for Biomedical Research, Emeryville, California 94608, United States;* Present Address: Via Nova Therapeutics, 1111 Broadway, Suite 1300, Oakland, CA, United States; orcid.org/0000-0002-1129-7618; Email: ben.taft@vianovatx.com

Fumiaki Yokokawa − *Global Discovery Chemistry, Novartis Institutes for Biomedical Research, Emeryville, California 94608, United States;* orcid.org/0000-0002-2861-9281; Email: fumiaki.yokokawa@novartis.com

Authors

Tom Kirrane − *Global Discovery Chemistry, Novartis Institutes for Biomedical Research, Emeryville, California 94608, United States*

Anne-Catherine Mata − *Global Discovery Chemistry, Novartis Institutes for Biomedical Research, Emeryville, California 94608, United States*

Richard Huang − *Global Discovery Chemistry, Novartis Institutes for Biomedical Research, Emeryville, California 94608, United States*

Nicole Blaquiere − *Global Discovery Chemistry, Novartis Institutes for Biomedical Research, Emeryville, California 94608, United States*

Grace Waldron − *Global Discovery Chemistry, Novartis Institutes for Biomedical Research, Emeryville, California 94608, United States*

Bin Zou − *Novartis Institute for Tropical Diseases, Singapore 138670, Singapore*

Oliver Simon − *Novartis Institute for Tropical Diseases, Singapore 138670, Singapore*

Subramanyam Vankadara − *Novartis Institute for Tropical Diseases, Singapore 138670, Singapore*

Wai Ling Chan − *Novartis Institute for Tropical Diseases, Singapore 138670, Singapore*

Mei Ding − *Novartis Institute for Tropical Diseases, Singapore 138670, Singapore*

Sandra Sim − *Novartis Institute for Tropical Diseases, Singapore 138670, Singapore*

Judith Straimer − *Novartis Institute for Tropical Diseases, Emeryville, California 94608, United States*

Armand Guiguemde − *Novartis Institute for Tropical Diseases, Emeryville, California 94608, United States*

Suresh B. Lakshminarayana − *Novartis Institute for Tropical Diseases, Emeryville, California 94608, United States*

Jay Prakash Jain − *Novartis Institute for Tropical Diseases, Emeryville, California 94608, United States*

Christophe Bodenreider − *Novartis Institute for Tropical Diseases, Singapore 138670, Singapore*

Christopher Thompson − *Novartis Institutes for Biomedical Research, Cambridge, Massachusetts 02139, United States*
Christian Lanshoeft − *Novartis Institutes for Biomedical Research, Basel CH-4056, Switzerland;* orcid.org/0000-0002-2405-0227
Wei Shu − *Global Discovery Chemistry, Novartis Institutes for Biomedical Research, Emeryville, California 94608, United States*
Eric Fang − *Chemical Biology and Therapeutics, Novartis Institutes for Biomedical Research, Emeryville, California 94608, United States*
Jafri Qumber − *Novartis Institute for Tropical Diseases, Emeryville, California 94608, United States*
Katherine Chan − *Novartis Institute for Tropical Diseases, Emeryville, California 94608, United States*
Luying Pei − *Novartis Institute for Tropical Diseases, Emeryville, California 94608, United States*
Yen-Liang Chen − *Novartis Institute for Tropical Diseases, Emeryville, California 94608, United States*
Hanna Schulz − *Novartis Institute for Tropical Diseases, Emeryville, California 94608, United States*
Jessie Lim − *Novartis Institute for Tropical Diseases, Singapore 138670, Singapore*
Siti Nurdiana Abas − *Novartis Institute for Tropical Diseases, Singapore 138670, Singapore*
Xiaoman Ang − *Novartis Institute for Tropical Diseases, Singapore 138670, Singapore*
Yugang Liu − *Technical Research and Development, Global Drug Development, Novartis Pharmaceuticals Corporation, East Hanover, New Jersey 07936, United States*
Iñigo Angulo-Barturen − *The Art of Discovery, Astondo Bidea, 48160 Bizkaia, Basque Country, Spain*
María Belén Jiménez-Díaz − *The Art of Discovery, Astondo Bidea, 48160 Bizkaia, Basque Country, Spain*
Francisco Javier Gamo − *Tres Cantos Medicines Development Campus, GlaxoSmithKline, Madrid 28760, Spain;* orcid.org/0000-0002-1854-2882
Benigno Crespo-Fernandez − *Tres Cantos Medicines Development Campus, GlaxoSmithKline, Madrid 28760, Spain*
Philip J. Rosenthal − *Department of Medicine, University of California, San Francisco, California 94143, Unites States*
Roland A. Cooper − *Department of Natural Sciences and Mathematics, Dominican University of California, San Rafael, California 94901, United States*
Patrick Tumwebaze − *Infectious Diseases Research Collaboration, Kampala, Uganda*
Anna Caroline Campos Aguiar − *São Carlos Institute of Physics, University of São Paulo, São Carlos, São Paulo 13563-120, Brazil*
Brice Campo − *Medicines for Malaria Venture, 1215 Geneva 15, Switzerland*
Simon Campbell − *Medicines for Malaria Venture, 1215 Geneva 15, Switzerland*
Jürgen Wagner − *Novartis Institute for Tropical Diseases, Singapore 138670, Singapore*
Thierry T. Diagana − *Novartis Institute for Tropical Diseases, Emeryville, California 94608, United States*
Christopher Sarko − *Global Discovery Chemistry, Novartis Institutes for Biomedical Research, Emeryville, California 94608, United States*

Complete contact information is available at: https://pubs.acs.org/10.1021/acs.jmedchem.1c01995

Funding
NITD thanks MMV for their generous support of this project. The Uganda isolates team thanks National Institutes of Health AI139179 and Medicines for Malaria Venture RD/15/0001.

Notes
The authors declare no competing financial interest.

■ ACKNOWLEDGMENTS

We acknowledge the synthetic contributions of our colleagues at WuXi AppTech, Aurigene Discovery Technologies, and Syngene. We are grateful to Prof. Rafael Guido, Dr. Dhelio Batista, Dr. Carolina Bioni, and Dr. Sergio Wittlin for contributions to *in vitro* studies. We are grateful to all associates at MMV and all partners within the MMV network. We are grateful to all associates at DiscoverX for contributions to kinase profiling. Special thanks to Mark Knapp for help with Haspin costructure figures. We also thank Heidi Struble, Alice Wang, Weiping Jia, and Shengtian Yang for the purification of the final compounds and analytical support. We are grateful to NITD Alliance Management and Partnering, Legal, and Finance team (Thomas Krucker, Mark Hopkins, Marcus Hall, and Jean Claude Poilevey) for their legal and financial support.

■ ABBREVIATIONS USED

acac, acetylacetonate; ADME, absorption, distribution, metabolism, and excretion; AUC, area under the curve; Boc_2O, di-*tert*-butyl dicarbonate; CL, clearance; DCM, dichloromethane; EC_{50}, half-maximal effective concentration; ED_{50}, effective dose 50; FaSSIF, fasted state simulated intestinal fluid; ITD, imidazothiadiazole; 2-MeTHF, 2-methyltetrahydrofuran; MMV, Medicines for Malaria Venture; MTBE, methyl *tert*-butyl ether; NIS, *N*-iodosuccinimide; NMP, *N*-methyl-2-pyrrolidone; $Pd(dppf)Cl_2 \cdot DCM$, [1,1′-bis-(diphenylphosphino)ferrocene]dichloropalladium(II), complex with dichloromethane; *Pf*, *Plasmodium falciparum*; PPB, plasma protein binding; RT, room temperature; SAR, structure−activity relationship; SCID, severe combined immunodeficiency; $T_{1/2}$, half-life; TMEDA, tetramethylethylenediamine; V_{ss}, volume steady state

■ REFERENCES

(1) WHO. *Malaria*. https://www.who.int/en/news-room/fact-sheets/detail/malaria (accessed 2021−05−01).
(2) Balikagala, B.; Fukuda, N.; Ikeda, M.; Katuro, O. T.; Tachibana, S. I.; Yamauchi, M.; Opio, W.; Emoto, S.; Anywar, D. A.; Kimura, E.; Palacpac, N. M. Q.; Odongo-Aginya, E. I.; Ogwang, M.; Horii, T.; Mita, T. Evidence of artemisinin-resistant malaria in Africa. *N Engl J. Med.* **2021**, *385*, 1163−1171.
(3) Rogers, W. O.; Sem, R.; Tero, T.; Chim, P.; Lim, P.; Muth, S.; Socheat, D.; Ariey, F.; Wongsrichanalai, C. Failure of artesunate-mefloquine combination therapy for uncomplicated Plasmodium falciparum malaria in southern Cambodia. *Malar. J.* **2009**, *8*, 10.
(4) Woodrow, C. J.; White, N. J. The clinical impact of artemisinin resistance in Southeast Asia and the potential for future spread. *FEMS Microbiol. Rev.* **2017**, *41*, 34−48.
(5) van der Pluijm, R. W.; Imwong, M.; Chau, N. H.; Hoa, N. T.; Thuy-Nhien, N. T.; Thanh, N. V.; Jittamala, P.; Hanboonkunupakarn, B.; Chutasmit, K.; Saelow, C.; Runjarern, R.; Kaewmok, W.; Tripura, R.; Peto, T. J.; Yok, S.; Suon, S.; Sreng, S.; Mao, S.; Oun, S.; Yen, S.; Amaratunga, C.; Lek, D.; Huy, R.; Dhorda, M.; Chotivanich, K.; Ashley, E. A.; Mukaka, M.; Waithira, N.; Cheah, P. Y.; Maude, R. J.;

Amato, R.; Pearson, R. D.; Goncalves, S.; Jacob, C. G.; Hamilton, W. L.; Fairhurst, R. M.; Tarning, J.; Winterberg, M.; Kwiatkowski, D. P.; Pukrittayakamee, S.; Hien, T. T.; Day, N. P.; Miotto, O.; White, N. J.; Dondorp, A. M. Determinants of dihydroartemisinin-piperaquine treatment failure in Plasmodium falciparum malaria in Cambodia, Thailand, and Vietnam: a prospective clinical, pharmacological, and genetic study. *Lancet Infect. Dis.* **2019**, *19*, 952−961.

(6) Rosenthal, P. J. Has artemisinin resistance emerged in Africa? *Lancet Infect. Dis.* **2021**, *21*, 1056−1057.

(7) Ramharter, M.; Kurth, F. M.; Belard, S.; Bouyou-Akotet, M. K.; Mamfoumbi, M. M.; Agnandji, S. T.; Missinou, M. A.; Adegnika, A. A.; Issifou, S.; Cambon, N.; Heidecker, J. L.; Kombila, M.; Kremsner, P. G. Pharmacokinetics of two paediatric artesunate mefloquine drug formulations in the treatment of uncomplicated falciparum malaria in Gabon. *J. Antimicrob. Chemother.* **2007**, *60*, 1091−1096.

(8) Burrows, J. N.; Duparc, S.; Gutteridge, W. E.; Hooft van Huijsduijnen, R.; Kaszubska, W.; Macintyre, F.; Mazzuri, S.; Mohrle, J. J.; Wells, T. N. C. New developments in anti-malarial target candidate and product profiles. *Malar. J.* **2017**, *16*, 26.

(9) White, N. J.; Pukrittayakamee, S.; Phyo, A. P.; Rueangweerayut, R.; Nosten, F.; Jittamala, P.; Jeeyapant, A.; Jain, J. P.; Lefevre, G.; Li, R.; Magnusson, B.; Diagana, T. T.; Leong, F. J. Spiroindolone KAE609 for falciparum and vivax malaria. *N. Engl. J. Med.* **2014**, *371*, 403−410.

(10) White, N. J.; Duong, T. T.; Uthaisin, C.; Nosten, F.; Phyo, A. P.; Hanboonkunupakarn, B.; Pukrittayakamee, S.; Jittamala, P.; Chuthasmit, K.; Cheung, M. S.; Feng, Y.; Li, R.; Magnusson, B.; Sultan, M.; Wieser, D.; Xun, X.; Zhao, R.; Diagana, T. T.; Pertel, P.; Leong, F. J. Antimalarial activity of KAF156 in falciparum and vivax malaria. *N. Engl. J. Med.* **2016**, *375*, 1152−1160.

(11) Llanos-Cuentas, A.; Casapia, M.; Chuquiyauri, R.; Hinojosa, J. C.; Kerr, N.; Rosario, M.; Toovey, S.; Arch, R. H.; Phillips, M. A.; Rozenberg, F. D.; Bath, J.; Ng, C. L.; Cowell, A. N.; Winzeler, E. A.; Fidock, D. A.; Baker, M.; Mohrle, J. J.; Hooft van Huijsduijnen, R.; Gobeau, N.; Araeipour, N.; Andenmatten, N.; Ruckle, T.; Duparc, S. Antimalarial activity of single-dose DSM265, a novel Plasmodium dihydroorotate dehydrogenase inhibitor, in patients with uncomplicated Plasmodium falciparum or Plasmodium vivax malaria infection: a proof-of-concept, open-label, phase 2a study. *Lancet Infect. Dis.* **2018**, *18*, 874−883.

(12) Sinxadi, P.; Donini, C.; Johnstone, H.; Langdon, G.; Wiesner, L.; Allen, E.; Duparc, S.; Chalon, S.; McCarthy, J. S.; Lorch, U.; Chibale, K.; Mohrle, J.; Barnes, K. I. Safety, tolerability, pharmacokinetics, and antimalarial activity of the novel Plasmodium phosphatidylinositol 4-kinase inhibitor MMV390048 in healthy volunteers. *Antimicrob. Agents Chemother.* **2020**, *64*, e01896−19.

(13) Gaur, A. H.; McCarthy, J. S.; Panetta, J. C.; Dallas, R. H.; Woodford, J.; Tang, L.; Smith, A. M.; Stewart, T. B.; Branum, K. C.; Freeman, B. B.; Patel, N. D.; John, E.; Chalon, S.; Ost, S.; Heine, R. N.; Richardson, J. L.; Christensen, R.; Flynn, P. M.; Van Gessel, Y.; Mitasev, B.; Möhrle, J. J.; Gusovsky, F.; Bebrevska, L.; Guy, R. K. Safety, tolerability, pharmacokinetics, and antimalarial efficacy of a novel Plasmodium falciparum ATP4 inhibitor SJ733: a first-in-human and induced blood-stage malaria phase 1a/b trial. *Lancet Infect. Dis.* **2020**, *20*, 964−975.

(14) McCarthy, J.; Yalkinoglu, O.; Odedra, A.; Webster, R.; Oeuvray, C.; Tappert, A.; Bezuidenhout, D.; Giddins, M.; Dhingra, S.; Fidock, D.; Marquart, L.; Webb, L.; Yin, X.; Khandelwal, A.; Bagchus, W. Safety, pharmacokinetics, and antimalarial activity of the novel Plasmodium eukaryotic translation elongation factor 2 inhibitor M5717: a first-in-human, randomised,placebo-controlled, double-blind, single ascending dose study and volunteer infection study. *Lancet Infect. Dis.* **2021**, *21*, 1713−1724.

(15) Hameed, S. P.; Solapure, S.; Patil, V.; Bharath, B.; Murugan, K.; Viswanath, P.; Puttur, J.; Srivastava, A.; Bellale, E.; Panduga, V.; Shanbag, G.; Awasthy, D.; Landge, S.; Morayya, S.; Koushik, K.; Saralaya, R.; Raichurkar, A.; Rautela, N.; Choudhury, N.; Ambady, A.; Nandishaiah, R.; Reddy, J.; Prabhakar, K. R.; Menasinakai; Suresh Rudrapatna, S.; Chatterji, M.; Bandodkar, B.; Mukherjee, K.; Balasubramanian, V.; Warner, P.; Hosagrahara, V.; Dudley, A.; Iyer, P.; Narayanan, S.; Sambandamurthy, V.; Henrich, P.; Coburn-Flynn, O.; Fidock, D.; Magistrado, P.; Lukens, A.; Wirth, D.; Jiménez-Díaz, M.; Martínez, M.; Sanz, L.; McLaughlin, R.; Waterson, D.; Rosenbrier-Ribeiro, L.; Hickling, K.; Kavanagh, S. Triaminopyrimidine is a fast-killing and long-acting antimalarial clinical candidate. *Nat. Commun.* **2015**, *6*, 6715.

(16) Avery, V. M.; Bashyam, S.; Burrows, J. N.; Duffy, S.; Papadatos, G.; Puthukkuti, S.; Sambandan, Y.; Singh, S.; Spangenberg, T.; Waterson, D.; Willis, P. Screening and hit evaluation of a chemical library against blood-stage *Plasmodium falciparum*. *Malar. J.* **2014**, *13*, 190.

(17) Pevarello, P.; García-Collazo, A. M.; García-García, A. B. Substituted imidazo (2,1-*b*)-1,3,4-thiazole compounds, their pharmaceutical compositions and uses thereof. WO 2009040552 A2, 2009.

(18) Pastor-Fernández, J.; García-Collazo, A. M.; Noya-Mariño, B.; González Cantalapiedra, E. Amino-imidazolothiadiazoles for use as protein or lipid kinase inhibitors WO 2012020217 A1, 2012.

(19) Assay performed as previously described: Aguiar, A. C. C.; Pereira, D. B.; Amaral, N. S.; De Marco, L.; Krettli, A. U. Plasmodium vivax and Plasmodium falciparum ex vivo susceptibility to antimalarials and gene characterization in Rondônia, West Amazon. *Brazil Malar. J.* **2014**, *13*, 73.

(20) Assay performed as previously described: Tumwebaze, P. K.; Katairo, T.; Okitwi, M.; Byaruhanga, O.; Orena, S.; Asua, V.; Duvalsaint, M.; Legac, J.; Chelebieva, S.; Ceja, F. G.; Rasmussen, S. A.; Conrad, M. D.; Nsobya, S. L.; Ozkan Aydemir, O.; Bailey, J. A.; Bayles, B. R.; Rosenthal, P. J.; Cooper, R. A. Drug susceptibility of Plasmodium falciparum in eastern Uganda: a longitudinal phenotypic and genotypic study. *Lancet Microbe.* **2021**, *2*, e441−e449.

(21) Linares, M.; Viera, S.; Crespo, B.; Franco, V.; Gómez-Lorenzo, M. G.; Jiménez-Díaz, M. B.; Angulo-Barturen, I.; Sanz, L. M.; Gamo, F.-J. Identifying rapidly parasiticidal anti-malarial drugs using a simple and reliable in vitro parasite viability fast assay. *Malar. J.* **2015**, *14*, 441.

(22) Sanz, L.; Crespo, B.; De-Cozar, C.; Ding, X.; Llergo, J.; Burrows, J.; Garcia-Bustos, J.; Gamo, F. J. P. falciparum in vitro killing rates allow to discriminate between different antimalarial mode-of-action. *PLoS One* **2012**, *7*, e30949.

(23) Karaman, M. W.; Herrgard, S.; Treiber, D. K.; Gallant, P.; Atteridge, C. E.; Campbell, B. T.; Chan, K. W.; Ciceri, P.; Davis, M. I.; Edeen, P. T.; Faraoni, R.; Floyd, M.; Hunt, J. P.; Lockhart, D. J.; Milanov, Z. V.; Morrison, M. J.; Pallares, G.; Patel, H. K.; Pritchard, S.; Wodicka, L. M.; Zarrinkar, P. P. A quantitative analysis of kinase inhibitor selectivity. *Nat. Biotechnol.* **2008**, *26*, 127−132.

(24) Jimenez-Díaz, M. B.; Mulet, V.; Viera, S.; Gomez, V.; Garuti, H.; Ibanez, J.; Alvarez-Doval, A.; Shultz, L. D.; Martínez, A.; Gargallo-Viola, D.; Angulo-Barturen, I. Improved murine model of malaria using Plasmodium falciparum competent strains and non-myelodepleted NOD-scid IL2Rgammanull mice engrafted with human erythrocytes. *Antimicrob. Agents Chemother.* **2009**, *53*, 4533−4536.

(25) Hultman, I.; Vedin, C.; Abrahamsson, A.; Winiwarter, S.; Darnell, M. Use of HμREL Human coculture system for prediction of intrinsic clearance and metabolite formation for slowly metabolized compounds. *Mol. Pharmaceutics* **2016**, *13*, 2796−2807.

(26) Hutzler, J. M.; Ring, B. J.; Anderson, S. R. Low-turnover drug molecules: A current challenge for drug metabolism scientists. *Drug Metab. Dispos.* **2015**, *43*, 1917−1928.

(27) Trager, W.; Jensen, J. B. Human malaria parasites in continuous culture. *Science* **1976**, *193*, 673−675.

(28) Johnson, J. D.; Dennull, R. A.; Gerena, L.; Lopez-Sanchez, M.; Roncal, N. E.; Waters, N. C. Assessment and continued validation of the malaria SYBR green I-based fluorescence assay for use in malaria drug screening. *Antimicrob. Agents Chemother.* **2007**, *51*, 1926−1933.

(29) Gubler, H.; Clare, N.; Galafassi, L.; Geissler, U.; Girod, M.; Herr, G. Helios: History and anatomy of a successful in-house enterprise high-throughput screening and profiling data analysis system. *SLAS Discovery* **2018**, *23*, 474−488.

https://doi.org/10.1021/acs.jmedchem.1c01995
J. Med. Chem. 2022, 65, 3798−3813